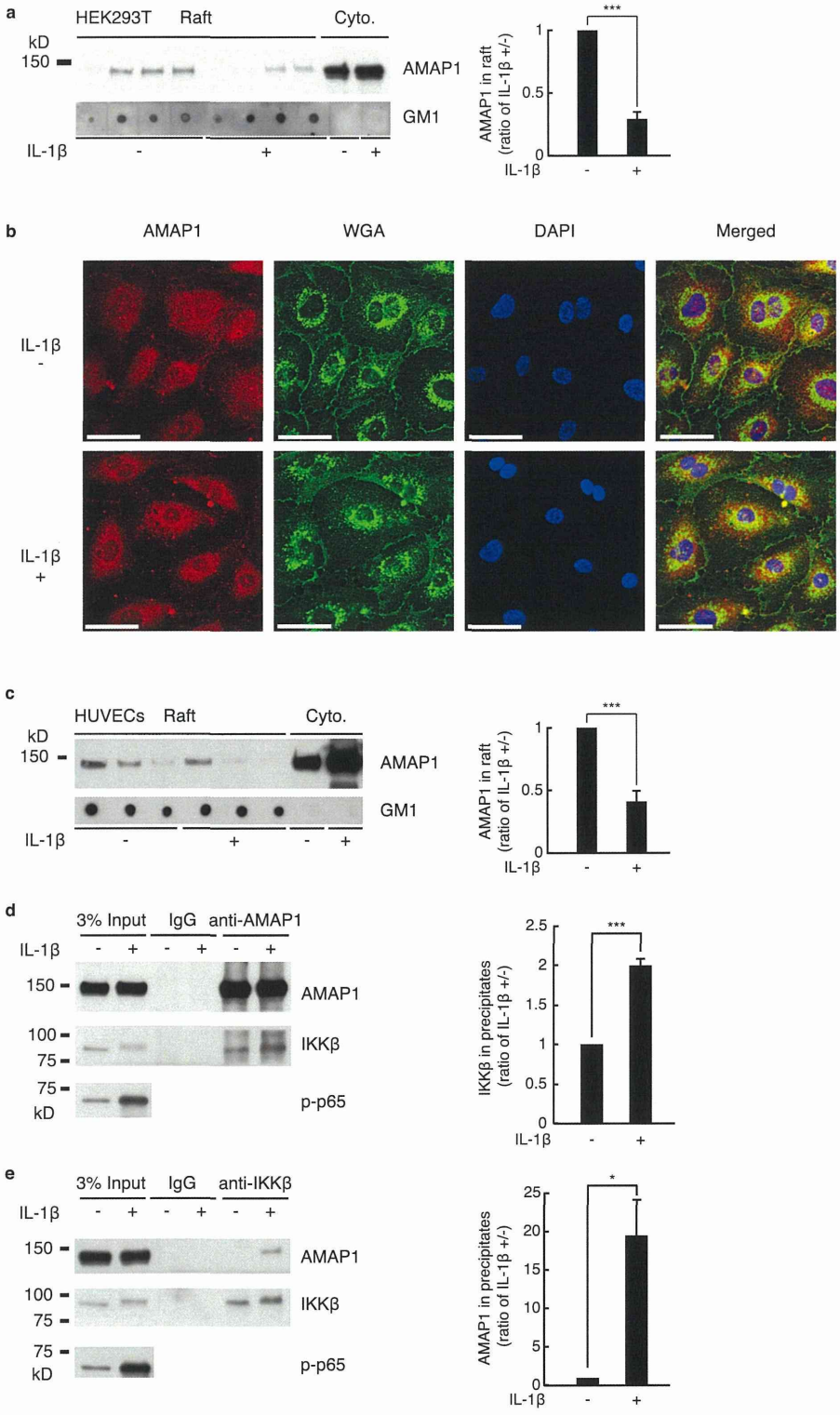

Figure 3 | IL-1β induces AMAP1 translocation and the AMAP1 and IKKβ interaction. (a) Representative AMAP1 immunoblots of fractions from sucrose gradient centrifugation of HEK293T cells treated with or without IL-1β (2.5 ng/mL) for 30 min and the cumulative, quantitative densitometry data from three independent experiments are shown. (b) HUVECs were treated with or without IL-1β (2.5 ng/mL) for 30 min and then stained with anti-AMAP1 antibody, WGA and DAPI (n = 3). Scale bar = 50 μm. (c) Representative AMAP1 immunoblots of fractions from sucrose gradient centrifugation of HUVECs treated with or without IL-1β (2.5 ng/mL) for 30 min and the cumulative, quantitative densitometry data from three independent experiments are shown. Representative blots from three immunoprecipitation experiments using anti-AMAP1 (d) and anti-IKKβ (e) antibodies in HUVECs treated with or without IL-1β (2.5 ng/mL) for 30 min. The graph represents the cumulative, quantitative densitometry data of the IKKβ blot in anti-AMAP1 antibody precipitates (d), of the AMAP1 blot in anti-IKKβ antibody precipitates (e). Error bar: ±SD. * $P < 0.05$, *** $P < 0.005$ in a two-sided, Student's *t*-test. Full-length blots are presented in Supplementary Figure 4.

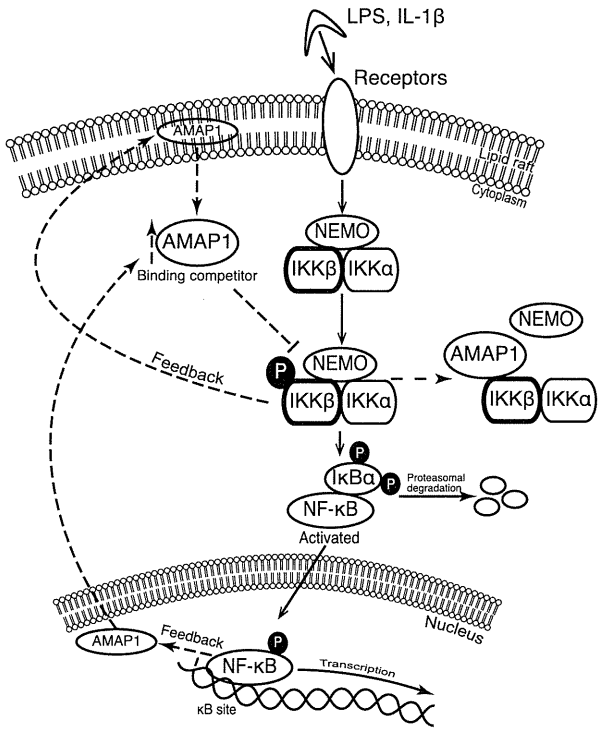

Figure 4 | Proposed model for AMAP1 as a binding protein of IKKβ and negative regulator of NF-κB. Dashed lines indicate the feedback mechanism.

radioresistance[7,9]. Considering the role of AMAP1 explored in this study, augmented expression of AMAP1 observed in cancer might indicate overwhelming NF-κB activation and self-repairing against cancer.

In summary, this study rediscovered AMAP1 as a negative regulator of NF-κB activity in a feedback mechanism, and AMAP1 could be a novel target for treatment or prevention against inflammatory diseases including cancer.

Methods

Reagents. The mammalian expression vectors that were used included pcDNA3.1-HA-AMAP1 and pcDNA3.1 as a control for AMAP1 overexpression, a series of mammalian expression vectors for IKKβ and its mutants (pIRES-AcGFP-hIKK2-WT, pIRES-AcGFP-hIKK2-Δ1, pIRES-AcGFP-hIKK2-Δ2, pIRES-AcGFP-hIKK2-Δ3 and pIRES-AcGFP-hIKK2-Δ4) and a series of mammalian expression vectors for AMAP1 and its mutants (pEBG/AMAP1-FL, pEBG/AMAP1-Bar, pEBG/AMAP1-PH, pEBG/AMAP1-ArfGAP, pEBG/AMAP1-ANK, pEBG/AMAP1-PRD and pEBG/AMAP1-SH3). The pcDNA3-HA-human-NEMO plasmid (Addgene plasmid 13512) to express NEMO was obtained from Professor Kunliang Guan (University of California, San Diego, USA)[34]. Small hairpin RNA (shRNA) expression constructs for silencing AMAP1 (shAMAP1) and control shRNA (shControl) were purchased from GeneCopoeia, Inc. (Rockville, MD, USA).

The antibodies that were used included anti-IKKβ (Millipore, Billerica, MA, USA); anti-AMAP1 (named anti-DDEF1, Santa Cruz Biotechnology, Dallas, Texas, USA); anti-HA (Sigma-Aldrich, St. Louis, MO, USA); monoclonal ANTI-FLAG® M2 (Sigma-Aldrich); a series of antibodies to anti-IKKβ, anti-phosphor-IκBα, anti-IκBα, anti-p65, anti-β-actin, anti-GAPDH, anti-TATA box-binding protein, anti-vimentin, anti-mouse IgG HRP-linked antibody and anti-rabbit IgG HRP-linked antibody (Cell Signaling Technology, Boston, MA, USA (CST)); anti-mouse IgG HRP and anti-rabbit IgG HRP (eBioscience, Inc. San Diego, CA, USA); Alexa Fluor 488 goat anti-rabbit IgG and Alexa Fluor 594 goat anti-mouse IgG (Invitrogen, Foster City, CA, USA); and Alexa Fluor 488 WGA. The reagents that were used included interleukin-1β (Wako Pure Chemical Industries, Ltd., Osaka, Japan (Wako)), LPS (Sigma-Aldrich) and NE-PER Nuclear and Cytoplasmic Extraction Reagents (Thermo Scientific, Rockford, IL, USA).

Cell culture. The human embryonic kidney 293T cell line (HEK293T) was maintained in DMEM (Wako) containing 10% FBS (Gibco, Foster City, CA, USA), 1% penicillin G/streptomycin (Sigma-Aldrich) at 37°C under 5% CO_2. Human umbilical vein endothelial cells (HUVECs) were maintained in Endothelial cell Basal Medium-2 (EBM-2) (Lonza, Basel, Switzerland) at 37°C under 5% CO_2.

Proteomics analysis. A Nano-LC/MALDI–TOF system was used with three types of IKKβ (wild-type IKKβ, a dominant-positive mutant of IKKβ and a dominant-negative mutant of IKKβ) that were overexpressed in HEK293T cells and immunoprecipitated by a specific antibody. Each sample was reduced with 45 mM of DTT (Wako), alkylated with 100 mM of iodoacetamide (Sigma-Aldrich) and digested with 2000 ng of trypsin (Promega, Madison, WI, USA). One-dimensional peptide fractionation was performed with a DiNa Direct Nano-Flow LC/MALDI system (KYA Tech., Tokyo, Japan) using a reverse-phase (RP) trap column (HiQ Sil C18-3, 0.8 mm i.d. × 3 mm) and an RP analytical column (HiQ Sil C18-3 Gradient, 0.15 mm i.d. × 50 mm). The peptides was subjected to the trap column and then to the analytical column using a gradient of 0–50% solvent B in solvent A over 65 minutes [solvent A: 0.1% trifluoroacetic Acid (TFA), 2% acetonitrile; solvent B: 0.1%TFA, 70% acetonitrile] followed by 50–100% solvent B for 15 minutes at a flow rate 200 nL/minute. The RP column eluent was spotted onto a MALDI sample plate using a DiNa Direct Nano-flow LC/MALDI system (KYA Tech.) and analyzed using a 4800 mass spectrometer (Applied Biosystems Inc., Foster City, CA, USA). The peptides were fragmented under collision-induced dissociation conditions to give fragment ions that produced sequence information for the peptide. The software packages used for data acquisition and analysis included GPS explorer (Applied Biosystems Inc.) and Mascot (Matrix Science, Boston, MA, USA), respectively. The parameters of tolerance for the searches were set to 100 ppm for the MS and 0.2 Da for the MS/MS analyses.

Co-immunoprecipitation (Co-IP). HEK293T cells (8×10^5) were cotransfected with 0.5 μg of AMAP1 plasmids and 0.5 μg of IKKβ plasmids using Effectene reagent (Qiagen, Valencia, CA, USA) according to the manufacturer's protocol. After 48 h, the cells were washed with PBS and lysed with Cell Lysis Buffer (CST). One milligram of the lysate was incubated with 1 μg of control IgG, anti-HA-tag or anti-FLAG antibody overnight at 4°C with agitation. Twenty-five microliters of protein G Sepharose (GE Healthcare, Uppsala, Sweden) was added, and the samples were rotated at 4°C for 1 h. The beads were washed three times with Cell Lysis Buffer and one time with Tris buffer pH 7.5. Proteins that were bound to the beads were eluted into SDS sample buffer, and the eluted material was analyzed by immunoblotting using anti-HA, anti-FLAG and anti-GST antibodies. Co-precipitation of endogenous AMAP1 with IKKβ was performed using anti-AMAP1 and anti-IKKβ antibodies.

Measurement of p65 activity. HEK293T cells were lysed with NE-PER Nuclear and Cytoplasmic Extraction Reagents (Thermo Scientific) for nuclear and cytoplasmic extractions. Transcription factor kits were used to detect the active NF-κB in the nuclear extract for NF-κB p65 according to the manufacturer's protocol. Briefly, the biotinylated NF-κB consensus sequence was bound to streptavidin-coated ELISA wells. Because only the active form of NF-κB (p65) binds to the DNA sequence, nonspecific binding was minimized. The p65 that was bound to the consensus sequence was incubated with anti-p65 antibody and then with a secondary, HRP-conjugated antibody. A chemiluminescent substrate was added to the wells, and the resulting signal was detected using a luminometer.

Sucrose gradient. Cells were treated with 5 ng/mL IL-1β or PBS for 30 min and lysed in cell lysis buffer (CST) containing 1 mM PMSF. An identical amount of protein from each sample was mixed with 90% sucrose in MES buffer (6 mL final volume, sucrose concentration 51.7–58.7%) and transferred to a Beckman ultracentrifuge tube. Four milliliters of 35% sucrose followed by 3 mL of 5% sucrose were overlaid, the samples were spun in a Beckman Coulter ultracentrifuge (39,000 rpm; approximately 180,000 × *g* in a SW40Ti rotor, 20 h), and 26 fractions were collected from the top of the gradient. For the detection of the lipid raft fractions, all fractions were dot-blotted with HRP-labeled cholera toxin B (Sigma-Aldrich) to detect Ganglioside GM1.

Immunofluorescence. HUVECs were grown on a 4-well chamber slide (Thermo Scientific) and treated with or without IL-1β 2.5 ng/mL for 30 min. The cells were washed with PBS, fixed with 4% paraformaldehyde and permeabilized with 0.5% Triton X-100. The cells were then incubated with blocking solution (5% goat normal serum in PBS) and labeled with anti-AMAP1 and anti-vimentin antibodies that were coupled to Alexa Fluor 488- and 584-conjugated secondary antibodies. The stained cells were mounted using Mounting Medium with DAPI (Vector Laboratories Inc., Burlingame, CA, USA). Images were captured and exported using a confocal microscope (Olympus FV1000; 60× oil-immersion lens, FLUOVIEW 3.0 software).

Statistical analysis. The data are presented as the mean of ±SD. Groups were compared using a two-tailed, Student's t-test. $P < 0.05$ was considered significant.

1. Oeckinghaus, A. & Ghosh, S. The NF-kappaB family of transcription factors and its regulation. *Cold Spring Harbor Perspect. Biol.* **1**, a000034, DOI:10.1101/cshperspect.a000034 (2009).
2. Karin, M. Nuclear factor-kappaB in cancer development and progression. *Nature* **441**, 431–436, DOI:10.1038/nature04870 (2006).

3. Rothwarf, D. M., Zandi, E., Natoli, G. & Karin, M. IKK-gamma is an essential regulatory subunit of the IkappaB kinase complex. *Nature* **395**, 297–300, DOI:10.1038/26261 (1998).
4. Mercurio, F. *et al.* IKK-1 and IKK-2: cytokine-activated IkappaB kinases essential for NF-kappaB activation. *Science* **278**, 860–866 (1997).
5. Li, Z. W. *et al.* The IKKbeta subunit of IkappaB kinase (IKK) is essential for nuclear factor kappaB activation and prevention of apoptosis. *J. Exp. Med.* **189**, 1839–1845 (1999).
6. Agarwal, A. *et al.* The AKT/I kappa B kinase pathway promotes angiogenic/metastatic gene expression in colorectal cancer by activating nuclear factor-kappa B and beta-catenin. *Oncogene* **24**, 1021–1031, DOI:10.1038/sj.onc.1208296 (2005).
7. Karin, M. NF-kappaB as a critical link between inflammation and cancer. *Cold Spring Harbor Perspect. Biol.* **1**, a000141, DOI:10.1101/cshperspect.a000141 (2009).
8. Jiang, R. *et al.* High expression levels of IKKalpha and IKKbeta are necessary for the malignant properties of liver cancer. *Int. J. Cancer* **126**, 1263–1274, DOI:10.1002/ijc.24854 (2010).
9. Chaturvedi, M. M., Sung, B., Yadav, V. R., Kannappan, R. & Aggarwal, B. B. NF-kappaB addiction and its role in cancer: 'one size does not fit all'. *Oncogene* **30**, 1615–1630, DOI:10.1038/onc.2010.566 (2011).
10. Ashida, N. *et al.* IKKbeta regulates essential functions of the vascular endothelium through kinase-dependent and -independent pathways. *Nat. Commun.* **2**, 318, DOI:10.1038/ncomms1317 (2011).
11. Furman, C., Short, S. M., Subramanian, R. R., Zetter, B. R. & Roberts, T. M. DEF-1/ASAP1 is a GTPase-activating protein (GAP) for ARF1 that enhances cell motility through a GAP-dependent mechanism. *J. Biol. Chem.* **277**, 7962–7969, DOI:10.1074/jbc.M109149200 (2002).
12. Inoue, H., Ha, V. L., Prekeris, R. & Randazzo, P. A. Arf GTPase-activating protein ASAP1 interacts with Rab11 effector FIP3 and regulates pericentrosomal localization of transferrin receptor-positive recycling endosome. *Mol. Biol. Cell.* **19**, 4224–4237, DOI:10.1091/mbc.E08-03-0290 (2008).
13. Liu, Y., Yerushalmi, G. M., Grigera, P. R. & Parsons, J. T. Mislocalization or reduced expression of Arf GTPase-activating protein ASAP1 inhibits cell spreading and migration by influencing Arf1 GTPase cycling. *J. Biol. Chem.* **280**, 8884–8892, DOI:10.1074/jbc.M412200200 (2005).
14. Randazzo, P. A. *et al.* The Arf GTPase-activating protein ASAP1 regulates the actin cytoskeleton. *Proc. Natl. Acad. Sci. U. S. A.* **97**, 4011–4016, DOI:10.1073/pnas.070552297 (2000).
15. Nam, J. M. *et al.* CIN85, a Cbl-interacting protein, is a component of AMAP1-mediated breast cancer invasion machinery. *Embo J.* **26**, 647–656, DOI:10.1038/sj.emboj.7601534 (2007).
16. Muller, T. *et al.* ASAP1 promotes tumor cell motility and invasiveness, stimulates metastasis formation in vivo, and correlates with poor survival in colorectal cancer patients. *Oncogene* **29**, 2393–2403, DOI:10.1038/onc.2010.6 (2010).
17. Onodera, Y. *et al.* Rab5c promotes AMAP1-PRKD2 complex formation to enhance beta1 integrin recycling in EGF-induced cancer invasion. *J. Cell. Biol.* **197**, 983–996, DOI:10.1083/jcb.201201065 (2012).
18. Hashimoto, S. *et al.* Requirement for Arf6 in breast cancer invasive activities. *Proc. Natl. Acad. Sci. U. S. A.* **101**, 6647–6652, DOI:10.1073/pnas.0401753101 (2004).
19. Onodera, Y. *et al.* Expression of AMAP1, an ArfGAP, provides novel targets to inhibit breast cancer invasive activities. *Embo J.* **24**, 963–973, DOI: 10.1038/sj.emboj.7600588 (2005).
20. Sabe, H., Onodera, Y., Mazaki, Y. & Hashimoto, S. ArfGAP family proteins in cell adhesion, migration and tumor invasion. *Curr. Opin. Cell. Biol.* **18**, 558–564, DOI:10.1016/j.ceb.2006.08.002 (2006).
21. Morishige, M. *et al.* GEP100 links epidermal growth factor receptor signalling to Arf6 activation to induce breast cancer invasion. *Nat. Cell. Biol.* **10**, 85–92, DOI:10.1038/ncb1672 (2008).
22. Boulay, P. L., Cotton, M., Melancon, P. & Claing, A. ADP-ribosylation factor 1 controls the activation of the phosphatidylinositol 3-kinase pathway to regulate epidermal growth factor-dependent growth and migration of breast cancer cells. *J. Biol. Chem.* **283**, 36425–36434, DOI:10.1074/jbc.M803603200 (2008).
23. Haque, A. *et al.* An ADP ribosylation factor-GTPase activating protein negatively regulates the production of proinflammatory mediators in response to lipopolysaccharide. *Cancer Immunol. Immunother.* **60**, 1439–1446, DOI:10.1007/s00262-011-1048-9 (2011).
24. Sabe, H. *et al.* The EGFR-GEP100-Arf6-AMAP1 signaling pathway specific to breast cancer invasion and metastasis. *Traffic* **10**, 982–993, DOI:10.1111/j.1600-0854.2009.00917.x (2009).
25. Xu, G. *et al.* Crystal structure of inhibitor of kappaB kinase beta. *Nature* **472**, 325–330, DOI:10.1038/nature09853 (2011).
26. May, M. J. *et al.* Selective inhibition of NF-kappaB activation by a peptide that blocks the interaction of NEMO with the IkappaB kinase complex. *Science* (New York, N.Y.) **289**, 1550–1554 (2000).
27. Lin, D. *et al.* ASAP1, a gene at 8q24, is associated with prostate cancer metastasis. *Cancer Res.* **68**, 4352–4359, DOI:10.1158/0008-5472.CAN-07-5237 (2008).
28. Birbach, A. *et al.* Signaling molecules of the NF-kappa B pathway shuttle constitutively between cytoplasm and nucleus. *J. Biol. Chem.* **277**, 10842–10851, DOI:10.1074/jbc.M112475200 (2002).
29. Verma, U. N., Yamamoto, Y., Prajapati, S. & Gaynor, R. B. Nuclear role of I kappa B Kinase-gamma/NF-kappa B essential modulator (IKK gamma/NEMO) in NF-kappa B-dependent gene expression. *J. Biol. Chem.* **279**, 3509–3515, DOI:10.1074/jbc.M309300200 (2004).
30. de Martin, R. *et al.* Cytokine-inducible expression in endothelial cells of an I kappa B alpha-like gene is regulated by NF kappa B. *Embo J.***12**, 2773–2779 (1993).
31. Haskill, S. *et al.* Characterization of an immediate-early gene induced in adherent monocytes that encodes I kappa B-like activity. *Cell* **65**, 1281–1289 (1991).
32. Sun, S. C., Ganchi, P. A., Ballard, D. W. & Greene, W. C. NF-kappa B controls expression of inhibitor I kappa B alpha: evidence for an inducible autoregulatory pathway. *Science* (New York, N.Y.) **259**, 1912–1915 (1993).
33. Pahl, H. L. Activators and target genes of Rel/NF-kappaB transcription factors. *Oncogene* **18**, 6853–6866, DOI:10.1038/sj.onc.1203239 (1999).
34. Tang, E. D. Negative Regulation of the Forkhead Transcription Factor FKHR by Akt. *J. Biol. Chem.* **274**, 16741–16746, DOI:10.1074/jbc.274.24.16741 (1999).

Acknowledgments

This work was performed under the Sponsored Research Program contracted between Kyoto University and Otsuka Pharmaceutical Co., Ltd., and was also supported by a Grant-in-Aid for Scientific Research from the Ministry of Education, Culture, Sports, Science and Technology of Japan. We also thank Prof. Kunliang Guan for the pcDNA3-HA-human-NEMO plasmid.

Author contributions

D.N.-T. and N.A. conceived and designed the research. D.N.-T., M.K., A.Y. and N.A. performed the experiments. A.Y. and A.H. made the constructs of AMAP1. H.S., E.N., K.K., H.A., T.K., T.K. and M.Y. supervised the project.

Additional information

Supplementary information accompanies this paper at http://www.nature.com/scientificreports

Competing financial interests: The authors declare no competing financial interests.

How to cite this article: Nguyen Tien, D. *et al.* AMAP1 as a negative-feedback regulator of nuclear factor-κB under inflammatory conditions. *Sci. Rep.* 4, 5094; DOI:10.1038/srep05094 (2014).

SCIENTIFIC REPORTS

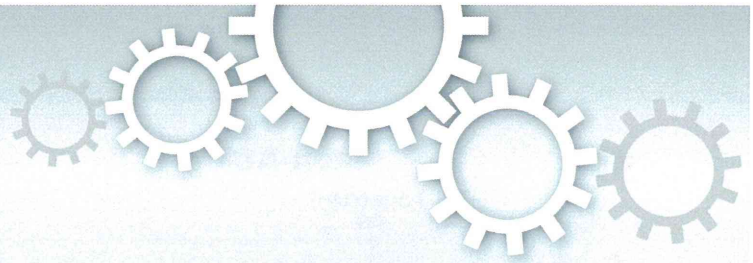

OPEN

SUBJECT AREAS:
PHOSPHOLIPIDS
BRAIN
MASS SPECTROMETRY
ALZHEIMER'S DISEASE

Received
10 July 2014

Accepted
4 November 2014

Published
20 November 2014

Correspondence and requests for materials should be addressed to M.S. (setou@hama-med.ac.jp)

DHA-PC and PSD-95 decrease after loss of synaptophysin and before neuronal loss in patients with Alzheimer's disease

Dai Yuki[1,2], Yuki Sugiura[1,3], Nobuhiro Zaima[1,4], Hiroyasu Akatsu[5,6], Shiro Takei[7,8], Ikuko Yao[7,8], Masato Maesako[9], Ayae Kinoshita[9], Takayuki Yamamoto[5], Ryo Kon[2], Keikichi Sugiyama[2,10] & Mitsutoshi Setou[1,8]

[1]Department of Cell Biology and Anatomy, Hamamatsu University School of Medicine, 1-20-1 Handayama, Higashi-ku, Hamamatsu, Shizuoka 431-3192, Japan, [2]Research and Development Headquarters, Lion Corporation, 7-2-1 Hirai, Edogawa-ku, Tokyo 132-0035, Japan, [3]JST Precursory Research for Embryonic Science Technology (PREST) Project, 160-8582 Tokyo, Japan, [4]Department of Applied Biological Chemistry, Kinki University, 3327-204 Naka-machi, Nara 631-8505, Japan, [5]Choju Medical Institute, Fukushimura Hospital, 19-14 Yamanaka, Noyori-cho, Toyohashi, Aichi 441-8124, Japan, [6]Department of Medicine for Aging in Place and Community-Based Medical Education, Nagoya City University Graduate School of Medical Sciences, Nagoya, Aichi 467-8601, Japan, [7]Department of Optical Imaging, Medical Photonics Research Center, Hamamatsu University School of Medicine, 1-20-1 Handayama, Higashi-ku, Hamamatsu, Shizuoka 431-3192, Japan, [8]JST, ERATO, Sato project, Tokyo 160-8582, Japan, [9]School of Human Health Sciences, Kyoto University Graduate School of Medicine, 53 Shogoin kawahara-cho, Sakyo-ku, Kyoto 606-8507, Japan, [10]Ritsumeikan Global Innovation Research Organization, Ritsumeikan University, 1-1-1 Nojihigashi, Kusatsu, Shiga 525-8577, Japan.

Alzheimer's disease (AD) is a progressive neurodegenerative disease that is characterized by senile plaques, neurofibrillary tangles, synaptic disruption, and neuronal loss. Several studies have demonstrated decreases of docosahexaenoic acid-containing phosphatidylcholines (DHA-PCs) in the AD brain. In this study, we used matrix-assisted laser desorption/ionization imaging mass spectrometry in postmortem AD brain to show that PC molecular species containing stearate and DHA, namely PC(18:0/22:6), was selectively depleted in the gray matter of patients with AD. Moreover, in the brain regions with marked amyloid β (Aβ) deposition, the magnitude of the PC(18:0/22:6) reduction significantly correlated with disease duration. Furthermore, at the molecular level, this depletion was associated with reduced levels of the postsynaptic protein PSD-95 but not the presynaptic protein synaptophysin. Interestingly, this reduction in PC(18:0/22:6) levels did not correlate with the degrees of Aβ deposition and neuronal loss in AD. The analysis of the correlations of key factors and disease duration showed that their effects on the disease time course were arranged in order as Aβ deposition, presynaptic disruption, postsynaptic disruption coupled with PC(18:0/22:6) reduction, and neuronal loss.

Alzheimer's disease (AD) is a progressive neurodegenerative disorder and the major cause of dementia in the elderly[1]. The main pathological hallmarks of AD are amyloid β (Aβ) plaques and hyperphosphorylated tau-containing neurofibrillary tangles[2–4]. Aβ is the leading candidate for the cause of neuronal loss and synaptic disruption, which causes the dementia in AD[5–7]

In the study of the postmortem brains of patients with AD, several researchers have reported that phosphatidylcholines (PCs) are decreased in patients with AD[8,9]. PCs, which are major lipid components in brain, can be subdivided into distinct molecular species depending on their composition of two fatty acids. In an analytical report of the molecular species of PCs, docosahexaenoic acid (DHA)-containing PCs (DHA-PCs) were significantly decreased in the brains of patients with AD[10]. In the central nervous system, DHA-PCs regulate the functioning of synaptic membrane-associated proteins because they affect membrane fluidity and protein-protein interactions[11,12]. DHA-PCs are also digested by Phospholipase A2 to produce free DHA and LysoPCs[13]. The oxidative products of free DHA, such as neuroprotectins, act as anti-apoptotic factors of neuronal cells[14]. Therefore, the decreases in DHA-PCs may be involved in the synaptic disruption and neuronal loss that occurs in AD.

The neuronal loss and synaptic disruption in AD are observed near Aβ deposition[15,16], and they have been reported to closely reflect the progression of the cognitive deficits in AD[17–19]. The neuronal loss in AD is most prominent in the temporal and frontal cortices[20], and the decreases in the levels of the presynaptic protein

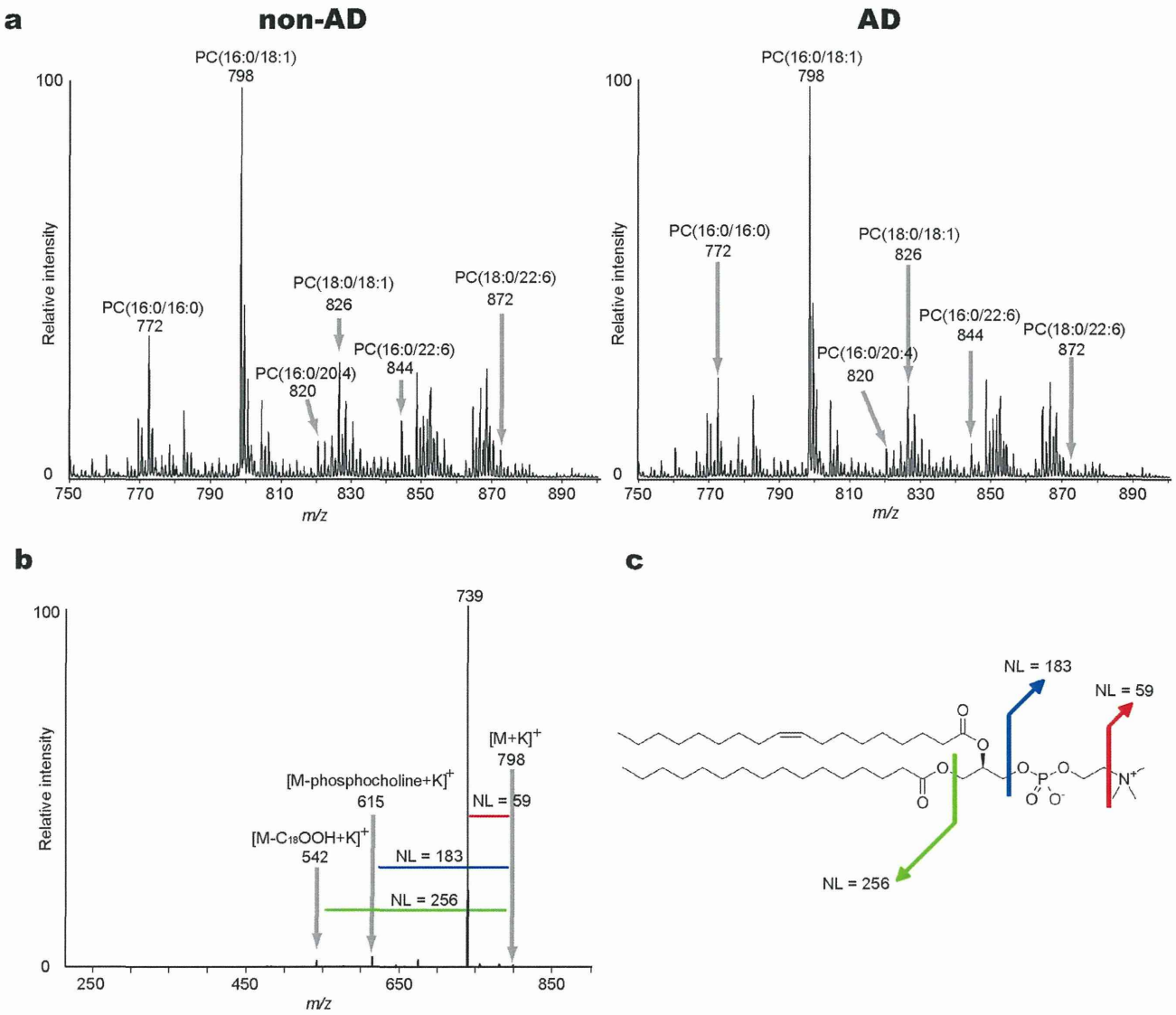

Figure 1 | Characterization of PC molecular species in the human brain by Matrix-Assisted Laser Desorption/Ionization-Tandem Mass Spectrometry (MALDI-MS/MS). (a) The averaged mass spectra from *m/z* 750 to 900 in non-Alzheimer's Disease (AD; left panel) and AD brains (right panel). The annotations indicate peak assignments to the phosphatidylcholine (PC) molecular species with different fatty acid compositions. (b) The tandem mass spectrum of PC(16:0/18:1) at *m/z* 798 as an example of the molecular characterization by this technique. The product ions at *m/z* 739 and *m/z* 615 (from loss of trimethylamine [NL 59] and phosphocholine [NL 183] residues, respectively), were commonly observed ions formed from the PC species. The product ion at *m/z* 542 was assigned to a fragment that was formed by the neutral loss of palmitic acid (16:0). (c) The panel shows the structural formula for PC(16:0/18:1) and the assignment of the cleavage positions. NL, neutral loss.

synaptophysin and the postsynaptic protein PSD-95, which reflect the synaptic disruption, are observed in the temporal and frontal cortices and the hippocampus[21–23]. The anatomical distribution of these substrates is important information in the study of neurodegeneration in patients with AD.

Here, we analyzed the distribution of DHA-PCs in the brain with Imaging Mass Spectrometry (IMS). IMS permits the direct analysis of biomolecules and the simultaneous visualization of the distribution of these molecules across a tissue section[24–26]. Matrix-Assisted Laser Desorption/Ionization (MALDI)-IMS, in particular, is practical for analytical lipid studies, and this method has revealed the distribution of PC species in mouse and human brain tissues[27–29]. With this technique, we analyzed the distributional changes of DHA-PCs in human brains with AD and in AD model mice and examined the association between DHA-PCs and aspects of neuronal loss and the decreases in synaptic proteins.

Results

The characterization of PC molecular species in the human brain. First, we characterized the PC molecular species in the human brain with MALDI-IMS (Fig. 1). For this purpose, we performed a structural analysis with tandem mass spectrometry (MS/MS) directly on the coronal brain tissue sections of patients with and without AD. As a result, we identified six mass peaks for PCs with distinct fatty-acid compositions in both AD and non-AD specimens.

The depletion of DHA-PC molecular species in the human temporal gray matter in MALDI-IMS. Next, we prepared coronal brain sections, including those from the frontal, parietal, and temporal lobes, for the imaging of the characterized PCs (Fig. 2). Fig. 2a shows Kluver-Barrera (KB)-stained sections and Aβ-immunostained sections. In the AD brain, high levels of Aβ deposition were observed in the gray matter. With continuous

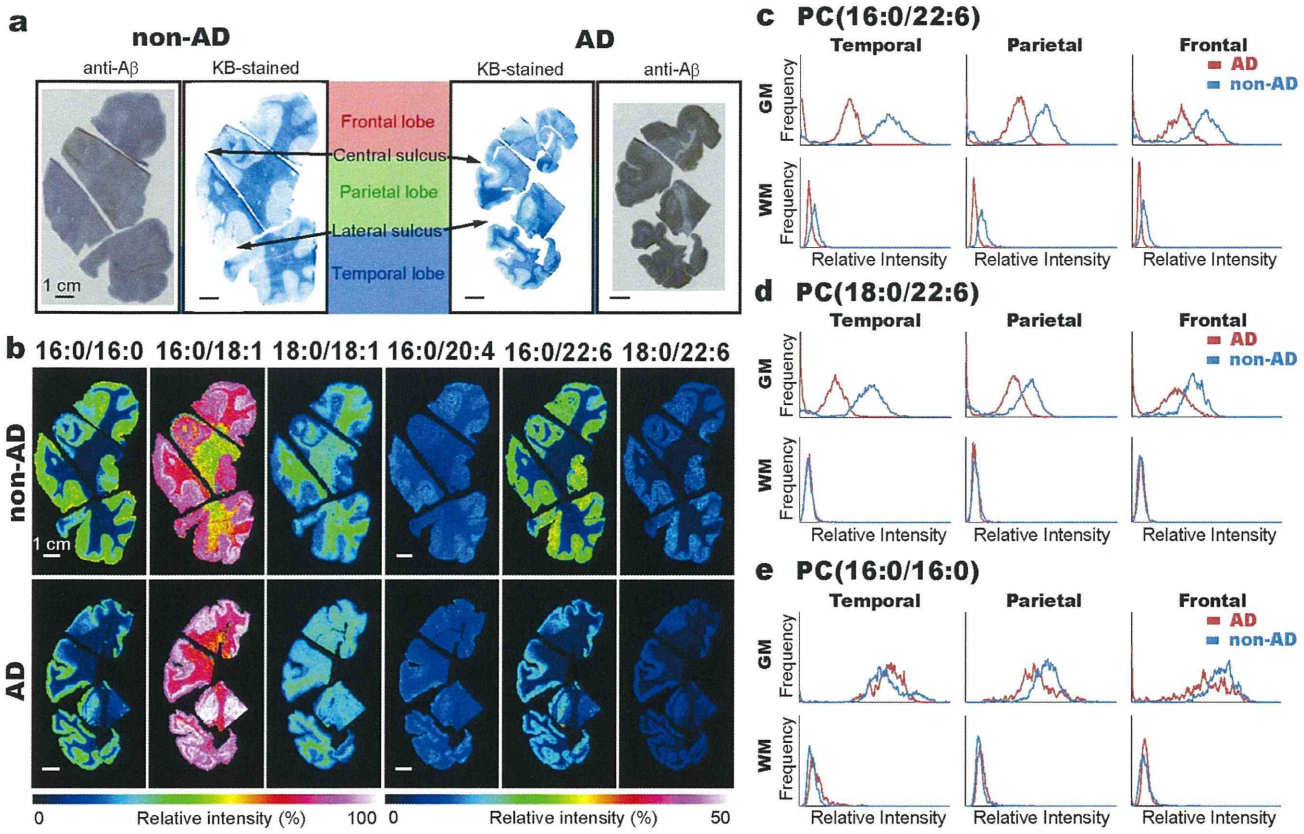

Figure 2 | Marked reduction of docosahexaenoic acid (DHA)-PC molecular species in the temporal gray matter in AD. (a) The pictures show Aβ-immunostained and Kluver-Barrera (KB)-stained coronal sections of non-AD and AD postmortem brains. (b) The distributions of the PC species in coronal sections of non-AD and AD brains that were analyzed by MALDI-imaging mass spectrometry (IMS) with 500-μm raster step sizes. The PCs with identical fatty acid moieties were arranged horizontally. The scale bars show 1 cm. (c–e) The graphs show the histograms of the intensity distributions of PC(16:0/22:6) (c), PC(18:0/22:6) (d), and PC(16:0/16:0) (e), in different brain regions in AD and non-AD brains from the relative intensity values of the MS images.

sections, we visualized the distribution of six PC molecular species with MALD-IMS (Fig. 2b). These images show that each PC has a distinct ion intensity difference between the gray and white matter regions. Although the distribution patterns of the PCs in the AD brain were similar to those in the non-AD brain, the ion intensities of the DHA-PC molecular species, such as PC(16:0/22:6) and PC(18:0/22:6), in the AD brain were lower than those in the non-AD brain. We then performed a more detailed analysis with histograms of the intensity distributions in different brain regions (Fig. 2c–e). In gray matter regions, the intensity distribution peaks of PC(16:0/22:6) and PC(18:0/22:6) shifted to lower values in the AD brain. In addition, the shifts were clearer in the temporal lobe. In white matter regions, however, the distribution peak of PC(16:0/22:6) slightly shifted lower in the AD brain, but PC(18:0/22:6) had similar distributions between the AD and non-AD brain.

PC(18:0/226) was markedly decreased in the gray matter in the human AD brains compared to other PC molecular species. With MALDI-IMS, we found that the ion intensities of DHA-PCs were decreased in the gray matter of the AD brains. To examine the repeatability and specificity of this result, we performed a liquid chromatography-electrospray ionization (LC-ESI) MS/MS analysis as an alternative quantitative method (Fig. 3) in the temporal lobes of nine non-AD and nine AD patients (Table 1). Fig. 3a shows the concentrations of all of the PCs in the gray matter and white matter regions of the non-AD and AD brains. Fig. 3b shows the changes in the concentrations of the PCs with the AD values as percentages of the non-AD values. All of the PCs were decreased both in the gray and white matter in the AD brains. In particular, PC(18:0/22:6) was decreased significantly in the gray matter. When investigating the compositional ratios of the PC species, we found that the ratio of PC(18:0/22:6) was clearly and specifically decreased in the gray matter (Fig. 3c). Therefore, both of the MALDI-IMS and LC-ESI MS/MS analyses showed a marked depletion of PC(18:0/22:6) in the temporal gray matter of the AD brains.

The compositional ratio of PC(18:0/22:6) correlated with disease duration. To further investigate the relationship of PC(18:0/22:6) to AD, we performed correlative analyses between the compositional ratio of PC(18:0/22:6) and Aβ density in the gray matter. Both factors correlated negatively in the analysis of the all-subjects group ($R = 0.545$, $P = 0.024$) but not in the analysis of the AD patients group ($R = 0.073$, $P = 0.781$) (Fig. 4a). We then examined the correlation with disease duration and found it to be negatively correlated with the compositional ratio of PC(18:0/22:6), both in the analysis of the all-subjects group ($R = 0.816$, $P = 0.001$) and in the analysis of the AD patients group ($R = 0.694$, $P = 0.002$) (Fig. 4b). However, the compositional ratio of PC(18:0/22:6) was not significantly correlated with the age at death in the all-subjects group ($R = 0.061$, $P = 0.817$) but was positively correlated with the age at death in the AD patients group ($R = 0.577$, $P = 0.015$) (Fig. 4c). The compositional ratio of PC(18:0/22:6) in proportion to disease duration was independent of the age of the subjects. In addition, the decrease in PC(18:0/22:6) was remarkable in patients with Braak Stage VI.

In this study, two cases of early-onset AD who had symptom onset before age 65 were included (Nos. 19 and 20 in Table 1). Because

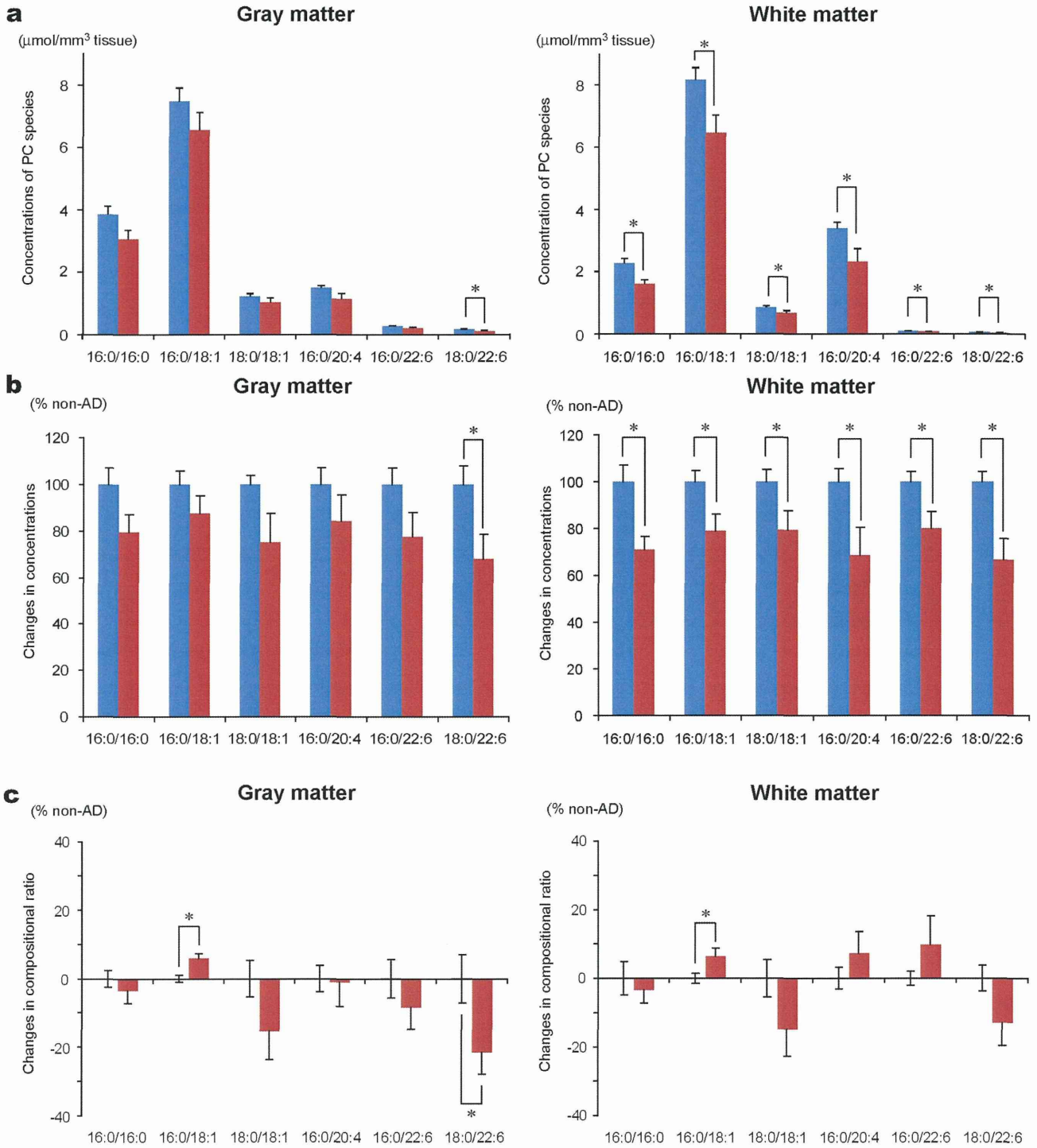

Figure 3 | Quantitative analyses of the PC species in non-AD and AD temporal lobe with liquid chromatography-electrospray ionization (LC-ESI) MS/MS. (a) The graphs show the concentrations of the PC species in the temporal gray (left panel) and white matter (right panel) of non-AD (blue bar) and AD (red bar) brains. (b) The graphs show the % changes of the PC concentrations between non-AD (blue bar) and AD (red bar) brains in the gray (left panel) and white matter (right panel). (c) The graphs show the % change of the PC composition ratio between the non-AD and AD brains in the gray (left graph) and white matter regions (right graph). The data are shown as mean [standard error (SE)]. n = 9, * $P < 0.05$.

early-onset patients generally show a more rapid clinical decline than late-onset patients[30], we also performed the correlation analyses in only the late-onset AD patients (n = 7). Even in the late-onset AD patients, the compositional ratio of PC(18:0/22:6) correlated with disease duration (R = 0.536, p = 0.027).

The compositional ratio of PC(18:0/22:6) correlated with PSD-95 expression in the AD brains but not with neuron density. We speculated that the observed depletion in PC(18:0/22:6) might be associated with neurodegenerative processes, such as neuronal loss and synaptic disruption, in gray matter regions of the AD brain. First,

Table 1 | Demographic data for patients with Alzheimer's disease (AD) and non-AD subjects

No.	Diagnosis	Gender	Age at death (years)	Duration of disease (years)	Braak stage	CERAD score	Postmortem interval (hours)	Clinical diagnosis
1	AD	male	80	10	VI	C	12	Alzheimer's disease, Dementia with Lewy bodies
2		female	83	9	VI	C	not recorded	Alzheimer's disease, Dementia with Lewy bodies
3		female	91	15	VI	C	20	Alzheimer's disease, Vascular dementia
4		female	93	7	VI	C	3	Alzheimer's disease, Cerebral amyloid angiopathy
5		female	91	4	V	C	18	Alzheimer's disease
6		male	81	11	VI	C	8	Alzheimer's disease, Acute respiratory failure
7		male	91	7	V	C	5	Alzheimer's disease
8		male	90	15	IV	C	not recorded	Alzheimer's disease, Progressive supranuclear palsy
9		female	86	28	VI	C	2	Alzheimer's disease, Cerebral amyloid angiopathy
10		female	75	23	VI	C	4	Alzheimer's disease
11	non-AD	male	88	0	I	0	20	hypoglycemia, pneumonia
12		male	79	0	I	B	13	multiple cerebral infarction
13		male	80	0	I	0	not recorded	multiple cerebral infarction
14		male	87	0	II	0	10	Cerebral infarction
15		female	82	0	I	0	34	Cerebral infarction
16		female	83	0	I	0	28	Phigiological aging
17		male	80	0	I	0	2	Phigiological aging
18		female	95	0	I	A	4	multiple cerebral infarction
19		female	86	0	II	A	4	multiple cerebral infarction
20		male	88	0	II	B	8	Cerebral infarction

Figure 4 | Correlations between the compositional ratio of PC(18:0/22:6) in the gray matter versus Aβ deposition, disease duration of AD, and age at death. (a) The compositional ratio of PC(18:0/22:6) in the gray matter plotted against Aβ deposition in non-AD and AD patients. (b) The compositional ratio of PC(18:0/22:6) in the gray matter plotted against the disease duration of AD in non-AD and AD patients. (c) The compositional ratio of PC(18:0/22:6) in the gray matter plotted against age at death in non-AD and AD patients. The left panels show analyses of all of the patients (non-AD and AD). The right panels show analyses of the AD patients only. A Pearson's test was used to determine the correlations between parameters. ■ = non-AD (n = 9); ◆ = AD (n = 9). The colors of the markers indicate the Braak stages of each subject as shown in the top-right box.

we examined the relationship between the decrease in PC(18:0/22:6) and neuron loss in the AD brain. Coronal temporal sections from non-AD and AD brains were immunostained with NeuN antibody, and the numbers of NeuN-positive nuclei were counted in the gray matter regions. The density of NeuN-positive nuclei in cortical layers II to VI in AD patients had a tendency to be less than those in non-AD patients. However, the density of NeuN-positive cells in the AD patients did not correlate with the compositional ratio of PC(18:0/22:6) (Fig. 5a, left panel), although the density of NeuN-positive cells negatively correlated with disease duration (Fig. 5a, right panel).

Second, we examined the relationship between PC(18:0/22:6) and synaptic disruption. We analyzed the expression levels of the presynaptic marker protein synaptophysin and the postsynaptic marker protein PSD-95 in the gray matter of non-AD and AD brains with immunoblotting (Fig. 5b). The protein levels for synaptophysin and PSD-95 were both decreased in the brains of AD patients. We then examined the correlations between the levels of synaptic proteins and the compositional ratio of PC(18:0/22:6) within the AD patients. A significant positive correlation was observed between PSD-95 and PC(18:0/22:6) ($R = 0.727$, $P = 0.001$), and no correlation was observed between synaptophysin and PC(18:0/22:6) ($R = 0.034$, $P = 0.898$) (Fig. 5c). The similar correlations were observed in the analyses within the late-onset AD patients; the compositional ratio of PC(18:0/22:6) correlated with the PSD-95 levels ($R = 0.491$, $p = 0.045$) but not with synaptophysin ($R = 0.275$, $p = 0.285$). We also examined the correlations between the synaptic protein levels and

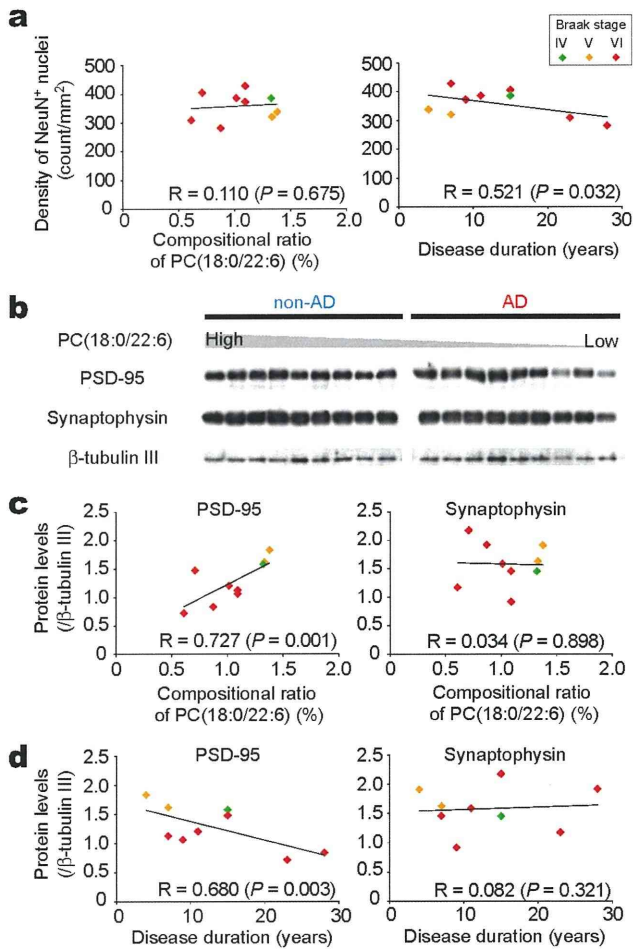

Figure 5 | A decrease in the PC(18:0/22:6) concentration correlates with PSD-95 expression but not synaptophysin expression or neuron density in AD. (a) The NeuN-positive density in the gray matter plotted against the compositional ratio of PC(18:0/22:6) (left panel) and disease duration (right panel) in AD (n = 9). The colors of the markers indicate the Braak stages of each patient as shown in the top-right box. (b) Shown are the western blot data for PSD-95, synaptophysin, and the internal standard β-tubulin III in the temporal gray matter of non-AD and AD brains. The lanes were arranged in descending order of the compositional ratio of PC(18:0/22:6) in non-AD and AD brains, respectively. (c) The compositional ratio of PC(18:0/22:6) in the gray matter plotted against the protein levels of PSD-95 (left panel) and synaptophysin (right panel) in AD brains (n = 9). (d) Disease duration plotted against the protein levels of PSD-95 (left panel) and synaptophysin (right panel) in AD brains (n = 9). A Pearson's test was used to determine the correlations between the parameters.

disease duration and found duration to be negatively correlated with PSD-95 (R = 0.680, P = 0.002) but not with synaptophysin (R = 0.082, P = 0.753) (Fig. 5d). In addition, we performed the correlational analyses between other synaptic proteins and PC(18:0/22:6) or disease duration, postsynaptic protein NR2B was strongly correlated with the PC(18:0/22:6) (R = 0.881, P = 0.001) and disease duration (R = 0.656, P = 0.004), and presynaptic protein Munc-18-1 was correlated with the PC(18:0/22:6) (R = 0.523, P = 0.031), but not with disease duration (R = 0.022, P = 0.932) (supplementary Fig. 1).

The compositional ratio of PC(18:0/22:6) was not decreased in the brains of 10-month-old APP-tg mice. Finally, to see if PC(18:0/22:6) was reduced at the Aβ-accumulating stage before the

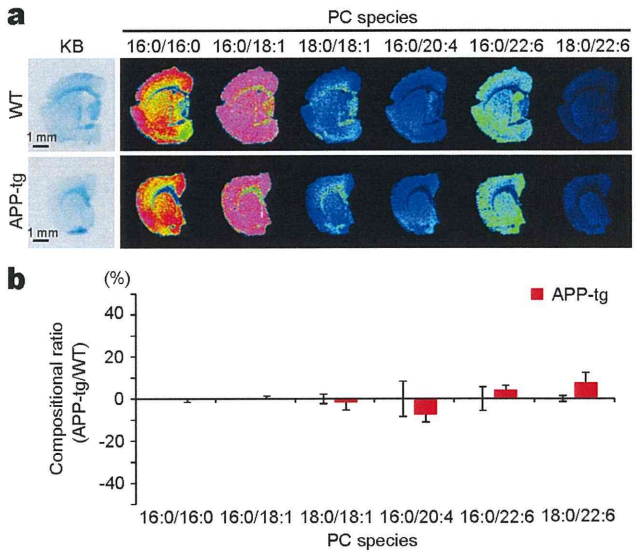

Figure 6 | The compositional ratio of PC(18:0/22:6) did not decrease in the brain of an Amyloid precursor protein-transgenic (APP-tg) mouse. (a) Shown are the KB-stained sections and mass spectrometry (MS) images of the PC species in serial coronal sections of APP-tg (J20) and wild-type (WT) mice. The MS images are shown with 50 μm spatial resolution. The scale bars show 1 mm. (b) The graphs show the % change in the PC composition ratio between the APP-tg and WT mice in the gray matter. The data are shown as mean (SE). n = 3.

postsynaptic disruptions, we performed a distributional analysis of PC in the brain of the human amyloid precursor protein (APP) transgenic (APP-tg) mouse (Fig. 6). Fig. 6a shows the distribution of the PC species in the coronal brain sections of 10-month-old APP-tg and wild-type (WT) mice. As was the case in the human brains, the distributions of the PCs in mice showed clearly different patterns between the gray and white matter, and PC(18:0/22:6) was distributed mainly in the gray matter. We did not find any significant differences in the contents of PC(18:0/22:6) in the gray matter of WT and APP-tg mice (Fig. 6b).

Discussion

In this study, we identified six PC species in the human brains that we examined with MALDI-IMS (Fig. 1). These six PC species were accounted for by approximately 70 mol% of the total PC in the human brain when we used the quantitative results for PC that have been reported by Hermansson et al. as a reference[31]. Therefore, our results indicated that MALDI-IMS is a useful tool for revealing the distributional changes in major PC metabolism in the human brain.

The MALDI-IMS study of cerebral coronal sections showed that the differences in the distributions of the PC species were mainly between gray and white matter (Fig. 2b). This was consistent with the findings of previous studies that used extraction methods and that showed that the fatty acid composition of PCs in the human brain is clearly different between gray and white matter[32]. In a more detailed analysis with histograms of the intensity distributions in different brain regions, PC(16:0/22:6) and PC(18:0/22:6) were markedly decreased in the temporal gray matter region in the AD brain (Fig. 2c and d). These imaging results indicated that a decrease in DHA-PCs might be associated with neurodegeneration in the temporal gray matter region.

Previous studies on postmortem AD brains have reported a decrease in the total amount of PC[8,9]. In our quantitative analysis with LC-ESI MS/MS, the amounts of all of the PC species were decreased in both the gray and white matter of the temporal lobe in the brains of patients with AD (Fig. 3a, b). After converting the

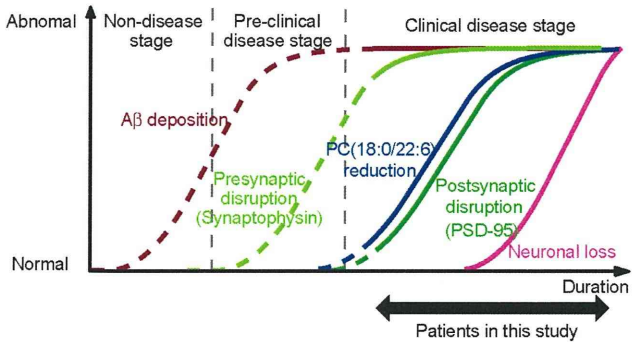

Figure 7 | Hypothetical cascade in AD progression. A PC(18:0/22:6) reduction parallels postsynaptic disruption when plotted against disease duration, but it does not parallel Aβ deposition, neuronal loss, and presynaptic disruption. It is generally accepted that Aβ deposition becomes abnormal early and before the appearance of clinical symptom, and the abnormal brain morphology resulting from neuronal loss happens late relative to neuronal dysfunction[31]. Because the loss of synaptophysin was not correlated with the disease durations of the patients in this study, presynaptic disruption may occur earlier than postsynaptic disruption. The solid lines show the results of this study, and the broken lines show our speculation.

quantitative data into compositional ratios of the PC species, only the ratio of PC(18:0/22:6) was significantly decreased in the gray matter region (Fig. 3c). Therefore, all of the PC species were decreased in both the gray and white matter, and PC(18:0/22:6) was markedly decreased in the gray matter of AD brains.

The present study showed that the decrease in PC(18:0/22:6) did not correlate with the levels of Aβ deposition in the AD patient group (Fig. 4a). Interestingly, the PC(18:0/22:6) concentration was negatively correlated with disease duration in the AD patients (Fig. 4b), but this was independent of the age of the patients (Fig. 4c). In addition, the decrease in PC(18:0/22:6) was remarkable in the patients with Braak stage VI. AD is a progressive neurodegenerative disease, and the clinical symptoms develop over years. In a recently developed model of the disease stages of AD, Aβ deposition became abnormal early before the neurodegeneration and the clinical symptoms occurred[33]. Moreover, the deposition did not correlate with cognitive impairment in AD[18]. However, the loss of neurons and the synaptic disruption happened later than the Aβ deposition[34], and they strongly correlated with the cognitive decline observed in AD[19,35]. Therefore, the progression of neurodegeneration is a more proximate pathological substrate of cognitive impairment in AD than Aβ deposition is[36]. Our result that the compositional ratio of PC(18:0/22:6) correlated with the duration of AD but not with Aβ deposition indicated that PC(18:0/22:6) was related to neurodegeneration in late-stage AD.

To examine the association with neurodegeneration in AD, we evaluated the possible relationship between the decrease in PC(18:0/22:6) and the loss of NeuN-positive cells (Fig. 5a). The density of NeuN-positive cells in AD brain did not correlate with a decrease in PC(18:0/22:6), but the density of the NeuN-positive cells negatively correlated with disease duration. These results indicated that the PC(18:0/22:6) reduction was not associated with neuronal loss. We next evaluated the relationship between the decrease in PC(18:0/22:6) and the loss of synaptic proteins (Fig. 5b). The postsynaptic protein PSD-95 was strongly correlated with PC(18:0/22:6) and disease duration (Fig. 5c and d). Similarly, the postsynaptic protein NR2B was strongly correlated with PC(18:0/22:6) and disease duration (Supplementary Fig. 1). However, the presynaptic protein synaptophysin did not correlate with PC(18:0/22:6) and disease duration, even though its levels were decreased in the AD brains. Although other presynaptic protein Munc-18-1 was correlated with PC(18:0/22:6), it did not correlate with disease duration (Supplementary Fig. 1). From these results, we hypothesized that the PC(18:0/22:6) was decreased at the clinical disease stage of AD and the reduction was more tightly associated with the postsynaptic disruptions than with the presynaptic disruptions (Fig. 7).

PSD-95 is a scaffold protein that is localized in postsynaptic terminals, and it has a critical role in postsynaptic function and plasticity[37–39]. A previous study with an AD mouse model (strain Tg2576) has reported that the loss of PSD-95 and other postsynaptic proteins is severe under a condition involving a dietary restriction of DHA, which has corresponding cognitive deficits[40]. Rodent studies have revealed that the brain's DHA content in phospholipids, such as PC, phosphatidylserine, and phosphatidylethanolamine, is decreased by dietary depletions of DHA[41,42]. However, a high DHA diet increases the DHA contents in the brain and increases the levels of PSD-95 and spine numbers[43,44]. Our results of the correlation of PC(18:0/22:6) and PSD-95 supported these previous studies and might indicate that PC(18:0/22:6) has an important role in the maintenance of postsynaptic function in humans.

Finally, we examined whether PC(18:0/22:6) was reduced at the early disease stage, which involves the accumulation of Aβ before postsynaptic disruption. We performed a MALDI-IMS analysis of brains from the 10-month-old AD model mouse J20 (Fig. 6) because J20 mice show Aβ deposition from the age of 8 months[45,46], and spine loss, which reflects active postsynaptic disruption, is observed after 11 months of age[47]. As a result, the distribution and composition level of PC(18:0/22:6) were not significantly different between 10-month-old J20 and WT mice. This result suggested that the decrease in PC(18:0/22:6) did not occur at the early disease stage along with Aβ deposition. In other words, Aβ deposition was not a direct cause of the decreases in PC(18:0/22:6) in the brain. In a recent study, oxidative stress has been postulated to be the major effector of synaptic dysfunction in the AD brain[48]. DHA is easily oxidized by free radicals due to its high enrichment in double bonds. Indeed, biochemical studies have demonstrated the increased concentrations of reactive products from DHA peroxidation in diseased regions of the AD brain[49]. The cause of the compositional decrease of PC(18:0/22:6) in the AD brain might be oxidative stress, and this may contribute to accelerating the postsynaptic disruption in AD.

In this study, we found that PC(18:0/22:6) was characteristically depleted in the gray matter regions of AD brains. This decrease in the PC(18:0/22:6) concentration was significantly correlated with disease duration and the loss of PSD-95 protein but not with Aβ deposition or the loss of synaptophysin. These findings implied that, in the clinical stage of the disease, the depletion of PC(18:0/22:6) was linked to postsynaptic disruption, which occurs after the presynaptic disruption and before the neuronal loss.

Methods

Human brain. Postmortem brains from 10 AD patients and 10 non-AD subjects were provided from the Choju Medical Institute, Fukushimura Hospital, Toyohashi, Japan (Table 1). All of the AD patients were diagnosed with AD from the clinical symptoms, the Braak stage, and the Consortium to Establish a Registry for Alzheimer's Disease score at Fukushimura Hospital. The brains were removed at autopsy and cut midsagittally, and the left hemispheres were coronally divided into several regions. The divided tissue blocks were frozen on dry ice and stored at −80°C. The study was performed in accordance with the guidelines for pathological specimen handling, which was approved by the ethical committee of the Choju Medical Institute and Hamamatsu University School of Medicine.

Animals. Human APP transgenic mice overexpressing the familial AD-linked mutations bearing both the Swedish (K670N/M671L) and Indiana (V717F) mutations (APP*Swe/Ind*)[45], which were imported from The Jackson Laboratory (Bar Harbor, ME, USA), were obtained from the Laboratory of the School of Human Health Science, Kyoto University. They were maintained as heterozygotes, and male and female mice were housed separately. These mice were age- and sex-matched (1:1, male:female) and maintained on a standard diet (10% fat, 70% carbohydrate, and 20% protein, Oriental Yeast Co., Ltd., Tokyo, Japan). The brains were extracted and cut sagittally into left and right hemispheres. After removing the olfactory lobe and

cerebellum, the right hemisphere was rapidly frozen in liquid nitrogen for the MALDI-IMS. All of the animal experiments were performed in compliance with the Guidelines for the Care and Use of Laboratory Animals of Kyoto University.

Preparation of the tissue samples for MALDI-IMS. For MALDI-IMS, we used the large brain blocks that included the frontal, parietal, and temporal lobes from one AD patient (No. 1, Table 1) and one non-AD subject (No. 11, Table 1), which was used as a control. The human brain coronal tissue block was divided into four small blocks. The divided human tissue blocks and mouse brains were sectioned at −19°C with a cryostat (CM 1950; Leica Biosystems GmbH, Nussloch, Germany) to a thickness of 8 μm, as described previously[27,50]. The frozen sections were thaw-mounted onto a MALDI plate (Bruker Daltonics GmbH, Leipzig, Germany) or indium-tin-oxide-coated glass slides.

Spray-coating with the matrix solution. A dihydroxybenzoic acid solution (50 mg/mL dihydroxybenzoic acid and 20 mM potassium acetate in methanol/water, 7:3, v/v) was used as the matrix solution. The matrix solution was sprayed over the tissue surface with a 0.2-mm caliber nozzle airbrush (Procon Boy FWA Platinum; Mr. Hobby, Tokyo, Japan). The distance between the nozzle tip and the tissue surface was maintained at 10 cm, and the spraying period was fixed at 5 min.

The molecular characterization of PC and visualization of its distribution. The molecular characterization was performed with MS/MS and a MALDI linear quadrupole ion-trap mass-spectrometer (Thermo Fisher Scientific Inc., Waltham, MA, USA). The MS/MS analysis was performed directly on the brain sections. The acquisition was in the mid-mass-range mode (m/z 100–1,000), which is the positive-ion detection mode, with an ionization voltage of 30 V and a collision voltage of 35 V. The PC molecular species were identified from the neutral loss compositions, which were determined from the deltas of the precursor and product ions in the MS/MS spectra.

The IMS of the identified PC species was performed with a MALDI time-of-flight (TOF)/TOF-type instrument (Ultraflex II TOF/TOF; Bruker Daltonics GmbH) that was equipped with a 355-nm Nd:YAG laser. The data were acquired in the positive-ion reflector mode under an accelerating potential of 20 kV. Calibration was performed with an external calibration method. The signals of m/z = 700–1,000 were measured. Raster scans on the tissue surfaces were performed automatically with FlexControl and FlexImaging 2.0 software (Bruker Daltonics GmbH). The number of laser irradiations was 200 shots per spot. Image reconstruction was performed with FlexImaging 2.0 software.

Sample preparation for LC-ESI MS/MS. For the LC-ESI MS/MS analysis, we analyzed the temporal lobes from the brains of nine AD patients (Nos. 2–10, Table 1) and nine non-AD subjects (Nos. 12–20, Table 1). The temporal lobes were sectioned at an 8-μm thickness and mounted on polymer-coated glass slides. Tissue sections with a 10-mm^2 area were microdissected from the gray and white matter regions with a Leica LMD6500 system (Leica Biosystems GmbH). The microdissected tissues were collected into microtubes, and 10 μL of an internal standard solution [1 mg/mL PC(20:1/20:1) in methanol] was added. The total lipids were extracted by the Folch method[51].

LC-ESI MS/MS analysis. The LC-ESI MS/MS analysis was performed with a 4000Q-TRAP quadrupole linear ion-trap hybrid mass spectrometer (Applied Biosystems/MDS SCIEX, Concord, ON, Canada) that was connected to an ACQUITY Ultra Performance Liquid Chromatography system (Waters Corporation, Milford, MA, USA). A chromatographic method was developed with an ACQUITY UPLC BEH C18 column (2.1 mm i.d. × 50 mm, 1.7 μm; Waters Corporation) that was fitted with an identically packed guard column (2.1 mm i.d. × 5 mm, 1.7 μm; Waters Corporation). The column oven was maintained at 40°C. A gradient elution was used with a mobile phase A (acetonitrile:methanol:water = 19:19:2 v/v/v containing 0.1% formic acid and 0.028% ammonia) and a mobile phase B (isopropanol containing 0.1% formic acid and 0.028% ammonia). The protocol was as follows: flow rate = 0.4 mL/min: 0–10 min: 5% B, 10–15 min: 5% B→50% B, 15–20 min: 50% B, 20–25 min: 50% B→5% B. The MS/MS analysis was performed in the positive ESI mode with the following settings: ion spray voltage, 5,500 kV and temperature, 600°C. The detection of specific PC species was performed by multiple reaction monitoring. The $[M + K]^+$ ions were selected in the first quadrupole (Q1) and collided with Ar in the second quadrupole (Q2) with a collision energy of 30 eV, and the product ions were detected at m/z 184 in the third quadrupole (Q3). The integrated signals of each monitored mass transition were corrected, and the signal of the internal standard PC(20 : 1/20 : 1) was used for quantification of each PC species.

Immunohistochemistry. The temporal lobes from the brains of the AD and non-AD subjects (Nos. 2–10 and 12–20, Table 1) were sectioned at −19°C with a cryostat (CM 1950; Leica Biosystems GmbH) at a thickness of 8 μm and thaw-mounted onto glass slides. The tissue sections were fixed with 4% paraformaldehyde/phosphate-buffered saline for 10 min at room temperature. The slides were incubated for 10 min in 100% ethanol containing 3% hydrogen peroxide to inactivate endogenous peroxidases. Nonspecific sites were blocked by a 1-h exposure to 10% bovine serum albumin in Tris-buffered saline (TBS). Incubations with the mouse anti-human amyloid beta antibody (clone 82E1, 1 : 100) or the mouse anti-NeuN antibody (clone A60, 1 : 1,000) were performed in 0.1% Tween-20 in 3% bovine serum albumin TBS for 1 h at room temperature. The secondary antibody was goat anti-mouse IgG (Histofine Simple Stain™ MULTI, Nichirei Biosciences Inc., Tokyo, Japan). After incubation with the secondary antibody and the ABC reagent (Thermo Fisher Scientific Inc., Rockford, IL, USA), sections were developed with metal-enhanced DAB kits (Thermo Fisher Scientific Inc.). Image analysis of the sections was performed with ImageJ software (NIH, Bethesda, MD, USA). The quantitative analysis of neuronal density (NeuN-positive cell count) was performed to produce an average in cortical layers II to VI.

Sample preparation for immunoblotting. The temporal lobe gray matter tissue from non-AD and AD patients (Nos. 2–10 and 12–20, Table 1) were homogenized in 10 volumes of lysis buffer (TBS, 1 mM ethylenediaminetetraacetic acid, 2% sodium dodecyl sulfate, 0.5% deoxycholate) containing a cocktail of protease inhibitors (complete and ethylenediaminetetraacetic acid-free, Roche Diagnostics, Indianapolis, IN, USA). The samples were sonicated briefly and centrifuged at 100,000 × g for 20 min at 4°C. The supernatants were subjected to immunoblotting.

Immunoblotting. Samples (20-μg protein) were electrophoresed on 10% acrylamide gels and transferred to polyvinylidene fluoride membranes (EMD Millipore Corporation, Billerica, MA). The membranes were blocked with TBS-T (0.1% Triton X-100 in TBS) containing 10% goat serum. The blot was rinsed with TBS-T and incubated at room temperature in TBS-T containing 2% goat serum and one of the following antibodies: anti-PSD-95 (clone K28/43, 1 : 100,000), anti-synaptophysin (clone SY38, 1 : 1,000), or anti-β-tubulin III (clone SDL.3D10, 1 : 1,000) for 90 min. Each membrane was then washed with TBS-T and incubated in TBS-T containing 2% goat serum and a 1 : 10,000 dilution of horseradish peroxidase-conjugated anti-mouse IgG for 60 min. Detection of the conjugated antibody was performed with ECL plus western blotting detection reagents (GE Healthcare Life Sciences, Freiburg, Germany). The fluorescence intensity of the immunoblotted proteins was quantified with ImageJ software and calibrated by using the β-tubulin III signal as an internal standard.

Statistical analysis. The data are presented as mean ± standard error. The statistical comparison of PC species levels between the AD and non-AD brains was performed with a Student's t-test. Differences were considered significant with p values less than 0.05. Pearson's test was used for the correlational analyses between the compositional ratio of PC(18:0/22:6) and Aβ deposition, disease duration, age at death, neuron density, and synaptic protein levels.

1. Jicha, G. A. & Carr, S. A. Conceptual evolution in Alzheimer's disease: implications for understanding the clinical phenotype of progressive neurodegenerative disease. *J. Alzheimers. Dis.* **19**, 253–272 (2010).
2. Braak, H. & Braak, E. Neuropathological stageing of Alzheimer-related changes. *Acta Neuropathol.* **82**, 239–259 (1991).
3. Mirra, S. S. *et al.* The Consortium to Establish a Registry for Alzheimer's Disease (CERAD). Part II. Standardization of the neuropathologic assessment of Alzheimer's disease. *Neurology* **41**, 479–486 (1991).
4. Selkoe, D. J. Aging, amyloid, and Alzheimer's disease: a perspective in honor of Carl Cotman. *Neurochem. Res.* **28**, 1705–1713 (2003).
5. Tomiyama, T. *et al.* A mouse model of amyloid beta oligomers: their contribution to synaptic alteration, abnormal tau phosphorylation, glial activation, and neuronal loss in vivo. *J. Neurosci.* **30**, 4845–4856 (2010).
6. Cavallucci, V., D'Amelio, M. & Cecconi, F. Aβ toxicity in Alzheimer's disease. *Mol. Neurobiol.* **45**, 366–378 (2012).
7. Ma, T. & Klann, E. Amyloid β: linking synaptic plasticity failure to memory disruption in Alzheimer's disease. *J. Neurochem.* **120**, 140–148 (2012).
8. Nitsch, R. M. *et al.* Evidence for a membrane defect in Alzheimer disease brain. *Proc. Natl. Acad. Sci. U S A* **89**, 1671–1675 (1992).
9. Pettegrew, J. W., Panchalingam, K., Hamilton, R. L. & McClure, R. J. Brain membrane phospholipid alterations in Alzheimer's disease. *Neurochem. Res.* **26**, 771–782 (2001).
10. Grimm, M. O. *et al.* From brain to food: analysis of phosphatidylcholins, lyso-phosphatidylcholins and phosphatidylcholin-plasmalogens derivates in Alzheimer's disease human post mortem brains and mice model via mass spectrometry. *J. Chromatogr. A.* **1218**, 7713–7722 (2011).
11. Stubbs, C. D. & Smith, A. D. The modification of mammalian membrane polyunsaturated fatty acid composition in relation to membrane fluidity and function. *Biochim. Biophys. Acta* **779**, 89–137 (1984).
12. Kim, H. Y. Novel metabolism of docosahexaenoic acid in neural cells. *J. Biol. Chem.* **282**, 18661–18665 (2007).
13. Burke, J. E. & Dennis, E. A. Phospholipase A2 biochemistry. *Cardiovasc. Drugs Ther.* **23**, 49–59 (2009).
14. Lukiw, W. J. *et al.* A role for docosahexaenoic acid-derived neuroprotectin D1 in neural cell survival and Alzheimer disease. *J. Clin. Invest.* **115**, 2774–2783 (2005).
15. Koffie, R. M. *et al.* Oligomeric amyloid beta associates with postsynaptic densities and correlates with excitatory synapse loss near senile plaques. *Proc. Natl. Acad. Sci. U S A* **106**, 4012–4017 (2009).
16. Meyer-Luehmann, M. *et al.* A reporter of local dendritic translocation shows plaque-related loss of neural system function in APP-transgenic mice. *J. Neurosci.* **29**, 12636–12640 (2009).
17. Gómez-Isla, T. *et al.* Neuronal loss correlates with but exceeds neurofibrillary tangles in Alzheimer's disease. *Ann. Neurol.* **41**, 17–24 (1997).

18. Giannakopoulos, P. *et al.* Tangle and neuron numbers, but not amyloid load, predict cognitive status in Alzheimer's disease. *Neurology* **60**, 1495–1500 (2003).
19. Scheff, S. W., Price, D. A., Schmitt, F. A., Scheff, M. A. & Mufson, E. J. Synaptic loss in the inferior temporal gyrus in mild cognitive impairment and Alzheimer's disease. *J Alzheimers Dis.* **24**, 547–557 (2011).
20. Cullen, K. M. *et al.* Cell loss in the nucleus basalis is related to regional cortical atrophy in Alzheimer's disease. *Neuroscience* **78**, 641–652 (1997).
21. Masliah, E. *et al.* Synaptic and neuritic alterations during the progression of Alzheimer's disease. *Neurosci. Lett.* **174**, 67–72 (1994).
22. Love, S. *et al.* Premorbid effects of APOE on synaptic proteins in human temporal neocortex. *Neurobiol. Aging* **27**, 797–803 (2006).
23. Sultana, R., Banks, W. A. & Butterfield, D. A. Decreased levels of PSD95 and two associated proteins and increased levels of BCl2 and caspase 3 in hippocampus from subjects with amnestic mild cognitive impairment: Insights into their potential roles for loss of synapses and memory, accumulation of Abeta, and neurodegeneration in a prodromal stage of Alzheimer's disease. *J. Neurosci. Res.* **88**, 469–477 (2010).
24. Patti, G. J. *et al.* Detection of carbohydrates and steroids by cation-enhanced nanostructure-initiator mass spectrometry (NIMS) for biofluid analysis and tissue imaging. *Anal. Chem.* **82**, 121–128 (2010).
25. Schwartz, S. A. & Caprioli, R. M. Imaging mass spectrometry: viewing the future. *Methods Mol. Biol.* **656**, 3–19 (2010).
26. Tucker, K. R., Li, Z., Rubakhin, S. S. & Sweedler, J. V. Secondary ion mass spectrometry imaging of molecular distributions in cultured neurons and their processes: comparative analysis of sample preparation. *J. Am. Soc. Mass Spectrom.* **23**, 1931–1938 (2012).
27. Sugiura, Y. *et al.* Visualization of the cell-selective distribution of PUFA-containing phosphatidylcholines in mouse brain by imaging mass spectrometry. *J. Lipid Res.* **50**, 1776–1788 (2009).
28. Matsumoto, J. *et al.* Abnormal phospholipids distribution in the prefrontal cortex from a patient with schizophrenia revealed by matrix-assisted laser desorption/ionization imaging mass spectrometry. *Anal. Bioanal. Chem.* **400**, 1933–1943 (2011).
29. Veloso, A. *et al.* Distribution of lipids in human brain. *Anal. Bioanal. Chem.* **401**, 89–101 (2011).
30. Jacobs, D. *et al.* Age at onset of Alzheimer's disease: relation to pattern of cognitive dysfunction and rate of decline. *Neurology* **44**, 1215–1220 (1994).
31. Hermansson, M. *et al.* Mass spectrometric analysis reveals changes in phospholipid, neutral sphingolipid and sulfatide molecular species in progressive epilepsy with mental retardation, EPMR, brain: a case study. *J. Neurochem.* **95**, 609–617 (2005).
32. O'Brien, J. S. & Sampson, E. L. Lipid composition of the normal human brain: gray matter, white matter, and myelin. *J. Lipid Res.* **6**, 537–544 (1965).
33. Jack, C. R. Jr. *et al* Hypothetical model of dynamic biomarkers of the Alzheimer's pathological cascade. *Lancet Neurol.* **9**, 119–128 (2010).
34. Sperling, R. A. *et al.* Toward defining the preclinical stages of Alzheimer's disease: recommendations from the National Institute on Aging-Alzheimer's Association workgroups on diagnostic guidelines for Alzheimer's disease. *Alzheimers. Dement.* **7**, 280–292 (2011).
35. Terry, R. D. *et al.* Physical basis of cognitive alterations in Alzheimer's disease: synapse loss is the major correlate of cognitive impairment. *Ann. Neurol.* **30**, 572–580 (1991).
36. Selkoe, D. J. Alzheimer's disease is a synaptic failure. *Science* **298**, 789–791 (2002).
37. El-Husseini, A. E., Schnell, E., Chetkovich, D. M., Nicoll, R. A. & Bredt, D. S. PSD-95 involvement in maturation of excitatory synapses. *Science* **290**, 1364–1368 (2000).
38. Vickers, C. A. *et al.* Neurone specific regulation of dendritic spines in vivo by post synaptic density 95 protein (PSD-95). *Brain Res.* **1090**, 89–98 (2006).
39. Radwanska, K. *et al.* Mechanism for long-term memory formation when synaptic strengthening is impaired. *Proc. Natl. Acad. Sci. U S A* **108**, 18471–18475 (2011).
40. Calon, F. *et al.* Docosahexaenoic acid protects from dendritic pathology in an Alzheimer's disease mouse model. *Neuron* **43**, 633–645 (2004).
41. Garcia, M. C., Ward, G., Ma, Y. C., Salem, N. Jr. & Kim, H. Y. Effect of docosahexaenoic acid on the synthesis of phosphatidylserine in rat brain in microsomes and C6 glioma cells. *J. Neurochem.* **70**, 24–30 (1998).
42. Hamilton, L., Greiner, R., Salem, N. Jr. & Kim, H. Y. n-3 fatty acid deficiency decreases phosphatidylserine accumulation selectively in neuronal tissues. *Lipids* **35**, 863–869 (2000).
43. Wurtman, R. J. *et al.* Synaptic proteins and phospholipids are increased in gerbil brain by administering uridine plus docosahexaenoic acid orally. *Brain Res.* **1088**, 83–92 (2006).
44. Sakamoto, T., Cansev, M. & Wurtman, R. J. Oral supplementation with docosahexaenoic acid and uridine-5'-monophosphate increases dendritic spine density in adult gerbil hippocampus. *Brain Res.* **1182**, 50–59 (2007).
45. Mucke, L. *et al.* High-level neuronal expression of abeta 1-42 in wild-type human amyloid protein precursor transgenic mice: synaptotoxicity without plaque formation. *J. Neurosci.* **20**, 4050–4058 (2000).
46. Maesako, M. *et al.* Environmental enrichment ameliorated high-fat diet-induced Aβ deposition and memory deficit in APP transgenic mice. *Neurobiol. Aging* **33**, 1011.e11–23 (2012).
47. Moolman, D. L., Vitolo, O. V., Vonsattel, J. P. & Shelanski, M. L. Dendrite and dendritic spine alterations in Alzheimer models. *J Neurocytol.* **33**, 377–387 (2004).
48. Ma, T. *et al.* Amyloid β-induced impairments in hippocampal synaptic plasticity are rescued by decreasing mitochondrial superoxide. *J. Neurosci.* **31**, 5589–5595 (2011).
49. Montine, K. S. *et al.* Isoprostanes and related products of lipid peroxidation in neurodegenerative diseases. *Chem. Phys. Lipids* **128**, 117–124 (2004).
50. Schwartz, S. A., Reyzer, M. L. & Caprioli, R. M. Direct tissue analysis using matrix-assisted laser desorption/ionization mass spectrometry: practical aspects of sample preparation. *J. Mass Spectrom.* **38**, 699–708 (2003).
51. Folch, J., Lees, M. & Sloane Stanley, G. H. A simple method for the isolation and purification of total lipides from animal tissues. *J. Biol. Chem.* **226**, 497–509 (1957).

Acknowledgments

This research was supported by a WAKATE-S, KIBAN-B, Lipid machinery grant from the Japan Society for the Promotion of Science (to Mitsutoshi Setou) and Platform grant, Center of Innovation grant from Ministry of Education, Culture, Sports, Science and Technology in Japan. We thank Dr. Yoshio Hashizume for neuropathological support.

Author contributions

D.Y., Y.S., N.Z., H.A., I.Y., R.K., K.S. and M.S. designed the experiments. D.Y., Y.S. and N.Z. performed the mass spectrometry experiments and data analysis. D.Y. and H.A. performed the immunostaining of the human brain sections. D.Y., S.T. and I.Y. performed the quantification of the synaptic proteins and statistical analyses. H.A. and T.Y. provided the human postmortem brains. M.M. and A.K. provided the transgenic mice. D.Y. and M.S. wrote the manuscript with help from Y.S., N.Z., H.A., I.Y., R.K. and K.S.

Additional information

Supplementary information accompanies this paper at http://www.nature.com/scientificreports

Competing financial interests: The authors declare no competing financial interests.

How to cite this article: Yuki, D. *et al.* DHA-PC and PSD-95 decrease after loss of synaptophysin and before neuronal loss in patients with Alzheimer's disease. *Sci. Rep.* **4**, 7130; DOI:10.1038/srep07130 (2014).

Journal of Alzheimer's Disease 45 (2015) 109–115
DOI 10.3233/JAD-142622
IOS Press

Idiopathic Normal Pressure Hydrocephalus has a Different Cerebrospinal Fluid Biomarker Profile from Alzheimer's Disease

Naoto Jingami[a,b], Megumi Asada-Utsugi[a,b], Kengo Uemura[a,b,c], Rio Noto[a], Makio Takahashi[d,e], Akihiko Ozaki[d,f], Takeshi Kihara[g], Takashi Kageyama[h], Ryosuke Takahashi[a], Shun Shimohama[i,*] and Ayae Kinoshita[b]

[a]*Department of Neurology, Kyoto University Graduate School of Medicine, Kyoto, Japan*
[b]*Department of Human Health Sciences, Kyoto University Graduate School of Medicine, Kyoto, Japan*
[c]*Department of Neurology, Ishiki Hospital, Kagoshima, Japan*
[d]*Department of Neurology, Osaka Saiseikai Nakatsu Hospital, Osaka, Japan*
[e]*Department of Neurology, Osaka Redcross Hospital, Osaka, Japan*
[f]*Department of Neurology, Kitano Hospital, Osaka, Japan*
[g]*Department of Neurology, Misasagi Hospital, Kyoto, Japan*
[h]*Department of Neurology, Tenri Yorozu Hospital, Nara, Japan*
[i]*Department of Neurology, Sapporo Medical University, Sapporo, Japan*

Accepted 12 November 2014

Abstract. The diagnosis of idiopathic normal pressure hydrocephalus (iNPH) is sometimes complicated by concomitant Alzheimer's disease (AD) pathology. The purpose of the present study is to identify an iNPH-specific cerebrospinal fluid (CSF) biomarker dynamics and to assess its ability to differentiate iNPH from AD. Total tau (t-tau), tau phosphorylated at threonine 181 (p-tau), amyloid-β (Aβ) 42 and 40, and leucine-rich α-2-glycoprotein (LRG) were measured in 93 consecutive CSF samples consisting of 55 iNPH (46 tap test responders), 20 AD, 11 corticobasal syndrome, and 7 spinocerebeller disease. Levels of t-tau and p-tau were significantly decreased in iNPH patients especially in tap test responders compared to AD. Correlation was observed between Mini-Mental State Examination scores and $A\beta_{42}$ in AD ($R = 0.44$) and mildly in iNPH ($R = 0.28$). Although $A\beta_{42/40}$ ratio showed no significant difference between iNPH and AD ($p = 0.08$), the levels of $A\beta_{40}$ and $A\beta_{42}$ correlated positively with each other in iNPH ($R = 0.73$) but much less in AD ($R = 0.26$), suggesting that they have discrete amyloid clearance and pathology. LRG levels did not differ between the two. Thus, our study shows that although CSF biomarkers of iNPH patients can be affected by concomitant tau and/or amyloid pathology, CSF t-tau and p-tau are highly useful for differentiation of iNPH and AD.

Keywords: Alzheimer's disease, amyloid-β, analysis of covariate, idiopathic normal pressure hydrocephalus, leucine-rich α-2-glycoprotein, Mini-Mental State Examination, tap test, tau phosphorylated at threonine 181, total tau

INTRODUCTION

Idiopathic normal pressure hydrocephalus (iNPH) is a neurological disease that usually develops in the elderly with a typical triad (i.e., gait instability, urinary incontinence, and cognitive dysfunction [1]). Neuroradiologically, iNPH is characterized by enlarged

*Correspondence to: Shun Shimohama, Department of Neurology, School of Medicine, Sapporo Medical University, Address: South 1, West 16, Chuo-ku, Sapporo 060-8543, Japan. Tel.: +81 11 611 2111; Fax: +81 11 622 7668; E-mail: shimoha@sapmed.ac.jp.

ventricles, widening of cortical sulci, and tightening of parasagittal upper convexity. Impairment of cerebrospinal fluid (CSF) clearance has been thought to be the main cause of the disease, and the symptoms can be alleviated by appropriate shunt surgery. Therefore, precise diagnosis of iNPH is of importance.

In practice, the diagnostic differentiation of iNPH from other neurodegenerative disorders can be difficult. For example, differentiating iNPH from Alzheimer's disease (AD) is difficult when the cognitive function of the patient is highly impaired. Cognitive impairment due to iNPH initially presents as frontal lobe dysfunctions with deficits in attention, execution, and thinking. In an advanced stage of iNPH, short-term memory is impaired like that in AD. In other instances, differentiating iNPH from neurobehavioral disorders, such as Parkinson's disease and corticobasal syndrome (CBS), can be challenging. The gait of iNPH patients is characterized by small-steps and magnet-like features, resembling the parkinsonian gait. Evaluating the efficacy of anti-parkinsonian drugs might be helpful for the diagnosis, but it is not always available. Some iNPH patients are reported to have coexisting AD pathology and sometimes CBS [2, 3]. In these cases, the efficacy of shunt surgery is limited and temporary, and surgical treatment cannot prevent the progressive clinical course of the comorbid diseases.

Tap test (TT) is useful for the diagnosis of iNPH, but the diagnosis is difficult in TT non-responders (NRs). Moreover, certain TT responders (Rs) undergone shunt surgery may still go through a progressive clinical course, despite the shunt surgery. The combination of neurological examination, neuroimaging study, and TT is sometimes not sufficient for a clear diagnosis. Additionally, quantitative estimates of overlapping AD pathology are almost impossible to assess with these clinical examinations. Thus, a biomarker is required in order to improve diagnostic accuracy and evaluation of iNPH.

Levels of total tau (t-tau), tau phosphorylated at threonine 181 (p-tau), and amyloid-β (Aβ) are so far established as CSF biomarkers for AD. In previous reports, the levels of t-tau and p-tau are elevated and the $A\beta_{42/40}$ ratio is decreased in CSF from AD patients [4–7]. On the other hand, an agreement on changes in CSF tau has not been established in iNPH patients. Previous studies show various results of CSF tau levels in iNPH in comparison to normal subjects: increased [8], decreased [9], and not changing [2]. However, CSF tau in iNPH patients is at least lower than that in AD. Another study showed that CSF $A\beta_{42}$ is also decreased in iNPH as in AD [8]. Further, leucine-rich α-2-glycoprotein (LRG) is reported to be highly elevated in iNPH and is believed to be an iNPH-specific candidate biomarker in CSF [10, 11].

Based on this evidence, we measured these CSF biomarkers and tried to find correlations between each biomarker level and the clinical symptoms in iNPH.

MATERIALS AND METHODS

Subjects

The study was undertaken in patients with iNPH, AD, and other neurodegenerative diseases. Participants were enrolled from 2009 to 2012 from four hospitals in Japan: Kyoto University Hospital (Hp.), Saiseikai Nakatsu Hp., Kitano Hp., and Tenri Yorozu Hp. A total of 93 consecutive CSF samples were collected in this study (55 iNPH, 20 AD, 11 CBS, and 7 spinocerebellar degeneration (SCD)). The demographics and clinical characteristics of subjects in each group are shown in Table 1.

Written informed consent for this study was obtained from each patient. Each patient underwent a standardized neurological evaluation. iNPH patients who fulfilled the diagnostic criteria of probable iNPH by the guidelines were selected including ventriculomegaly with Evans index (EI) >0.3 on a computed tomography imaging study [12]. All of the iNPH patients underwent TT, and TT Rs was defined as one whose walking speed increased more than 10%. Those who did not respond were defined as NRs. Among the 55 iNPH patients, 46 (83.6%) were Rs (Table 1). An AD diagnosis was based on current international clinical criteria [13]. Each iNPH and AD patient was scored with the Mini-Mental State Examination (MMSE).

Biomarker levels in CSF samples (t-tau, p-tau, $A\beta_{42/40}$ ratio, LRG)

Levels of t-tau, p-tau, $A\beta_{42/40}$ ratio, and LRG in the CSF were measured with an enzyme-linked immunosorbent assay according to the manufacturer's protocol; Tau (Total) Human ELISA Kit - Novex, Phospho-Tau (181P) - Innotest, Human Amyloid β (1-42) Assay Kit - IBL, Human Amyloid β (1-40) Assay Kit - IBL, and Human LRG Assay Kit - IBL.

Statistical analyses

Comparisons among groups were performed using Chi-square test. Analysis of covariance (ANCOVA) was additionally used to compare the levels of each

Table 1
Demographic characteristics and CSF biomarker scores of the sample groups

	iNPH	*iNPH Rs*	*iNPH NRs*	AD	CBS	SCD	p_1 (iNPH versus AD)
n	55	46	9	20	11	7	
Age (y)[c]	76.4 (7.2)	76.6 (7.5)	75.4 (5.5)	71.8 (12.8)	71.7 (6.7)	70.4 (12.6)	0.051[a]
MMSE[c]	23.6 (4.9)	23.5 (5.2)	24.4 (3.3)	18.9 (6.1)	24.0 (3.5)	26.4 (3.9)	0.001[a]
EI[c]	0.34 (0.04)	0.33 (0.04)	0.35 (0.04)				
t-tau (pg/ml)[d]	297 (232–440)	297 (220–398)	455 (376–682)	932 (716–1533)	487 (353–737)	513 (400–766)	<0.0001[a], <0.0001[b]
p-tau (pg/ml)[d]	16.0 (11.3–23.7)	15.7 (11.3–21.5)	17.8 (14.2–40.1)	57.0 (32.1–102)	26.1 (22.7–27.1)	NA	<0.0001[a], <0.0001[b]
$A\beta_{42/40}$[d]	0.055 (0.045–0.062)	0.054 (0.044–0.061)	0.059 (0.054–0.064)	0.038 (0.029–0.055)	0.046 (0.035–0.051)	0.058 (0.047–0.061)	<0.01[a], 0.08[b]
LRG (ng/ml)[d]	33.8 (30.2–37.0)	33.2 (29.1–35.6)	34.8 (33.0–37.3)	33.0 (28.5–34.2)	30.1 (29.7–34.6)	32.0 (28.3–36.8)	0.22[a], 0.56[b]

iNPH, idiopathic normal pressure hydrocephalus; Rs, responders; NRs, non-responders; AD, Alzheimer's disease; CBS, corticobasal syndrome; SCD, spinocerebellar degeneration; MMSE, Mini-Mental State Examination; EI, Evans index; t-tau, total tau; p-tau, phosphorylated tau; Aβ, amyloid-β; LRG, leucine-rich α-2-glycoprotein; NA, not analyzed; P_1, comparison between iNPH and AD. [a] χ^2 test, [b]ANCOVA after MMSE transformation, [c]Mean and SD, [d]median value (25th–75th percentile).

biomarker between iNPH and AD on assessments after adjustment for each individual MMSE score. Optimal sensitivity and specificity of each biomarker were determined by the receiver operating characteristic (ROC) curve analysis. Results are indicated as median and 25th–75th percentile. Statistical significance was defined at $p < 0.05$.

RESULTS

The CSF biomarker scores of each group are shown in Fig. 1 and Table 1. ROC analysis results of each biomarker for differentiating iNPH from AD are shown in Fig. 2 and Table 2.

Levels of t-tau and p-tau (pg/ml) were significantly lower in iNPH patients than those in AD patients ($p < 0.0001$, $p < 0.0001$, respectively) (Fig. 1a, b). These differences had great deals of diagnostic accuracies, with the area under the curves (AUC) 0.90 and 0.91, with optimal threshold values of 766 (sensitivity 75%, specificity 98%) and 24.4 (sensitivity 95%, specificity 74%), respectively (Fig. 2). In the iNPH patients, levels of t-tau and p-tau were lower in the Rs subgroup than in the NRs subgroup ($p < 0.05$, $p = 0.06$, respectively). Levels of t-tau in Rs were lowest with significance compared with rest of the groups (Fig. 1a, b). The levels of t-tau and p-tau strongly correlated with each other in AD (R = 0.90) and iNPH NRs (R = 0.91)

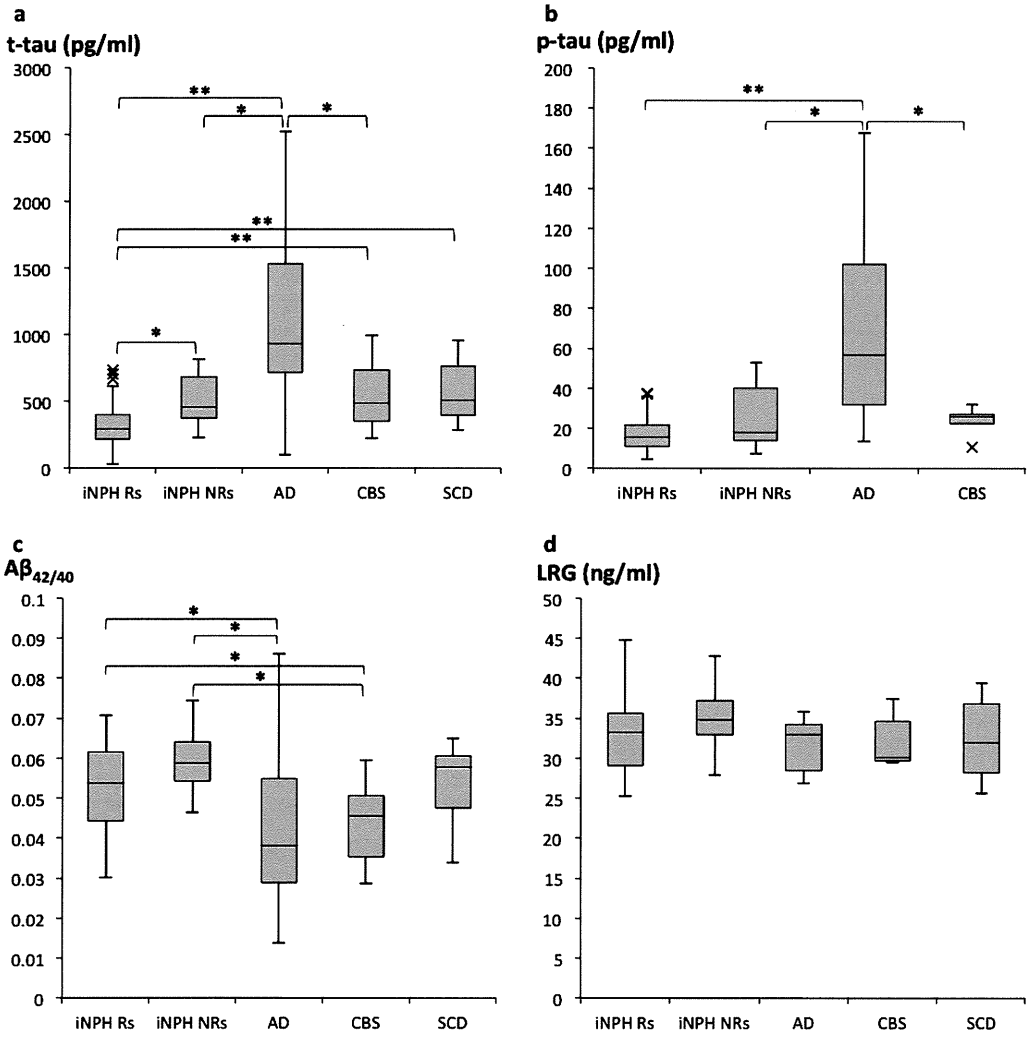

Fig. 1. Box plots of each CSF biomarker in the studied group; t-tau (a), p-tau (b), $A\beta_{42/40}$ ratio (c), and LRG (d). Horizontal lines within boxes show median values, boxes show upper and lower interquartile (IQ) ranges, whiskers indicate the 1.5 times IQ, a cross (x) in the figure indicate outlier values (1.5 times IQ). $^{*}p < 0.05$, $^{**}p < 0.001$.

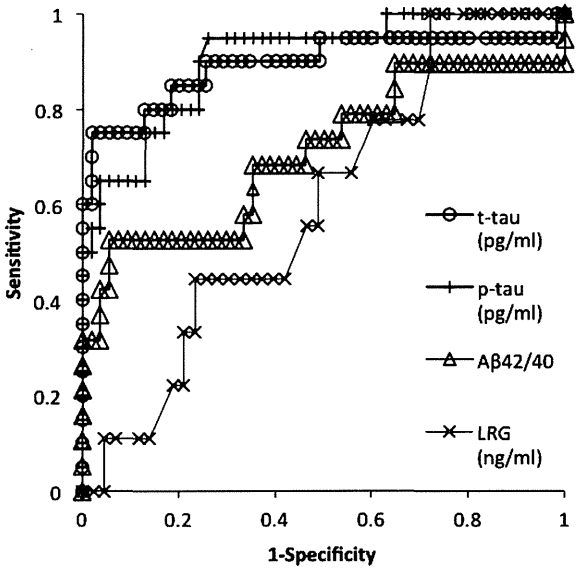

Fig. 2. ROC curve analysis for each CSF biomarker for differentiation of iNPH from AD.

Table 2
Comparison of CSF biomarkers between patients with iNPH and AD: ROC analysis

	t-tau	p-tau	$A\beta_{42/40}$	LRG
AUC	0.90	0.91	0.71	0.60
Cutoff value	766 pg/ml	24.4 pg/ml	0.038	35.8 ng/ml
Sensitivity	75%	95%	53%	100%
Specificity	98%	74%	94%	28%

iNPH, idiopathic normal pressure hydrocephalus; AD, Alzheimer's disease; t-tau, total tau; p-tau, phosphorylated tau; Aβ, amyloid-β; LRG, leucine-rich α-2-glycoprotein; ROC, receiver operating characteristic analysis; AUC, area under the curve.

subgroups compared to iNPH Rs (R = 0.54) subgroup (Fig. 3a).

The $A\beta_{42/40}$ ratio was higher in iNPH patients than in AD patients ($p < 0.01$). Using ANCOVA with diagnostic group of iNPH and AD as a factor, and MMSE scores as a covariate, the diagnostic group did not show impact on the levels of $A\beta_{42/40}$ ratio ($p = 0.08$) (Fig. 1c, Table 1). MMSE scores of AD patients were correlated with the levels of $A\beta_{42}$ (R = 0.44) and inversely correlated to the levels of t-tau (R = 0.37), whereas the iNPH group showed less clear correlations between MMSE scores and the levels of $A\beta_{42}$ (R = 0.28). In iNPH group, MMSE scores and the levels of t-tau were not inversely correlated as in AD (R = 0.17) (Fig. 4a, b). The levels of $A\beta_{40}$ and $A\beta_{42}$ showed strong correlations in the iNPH (R = 0.73) and CBS (R = 0.94) groups, while they showed less clear correlation in

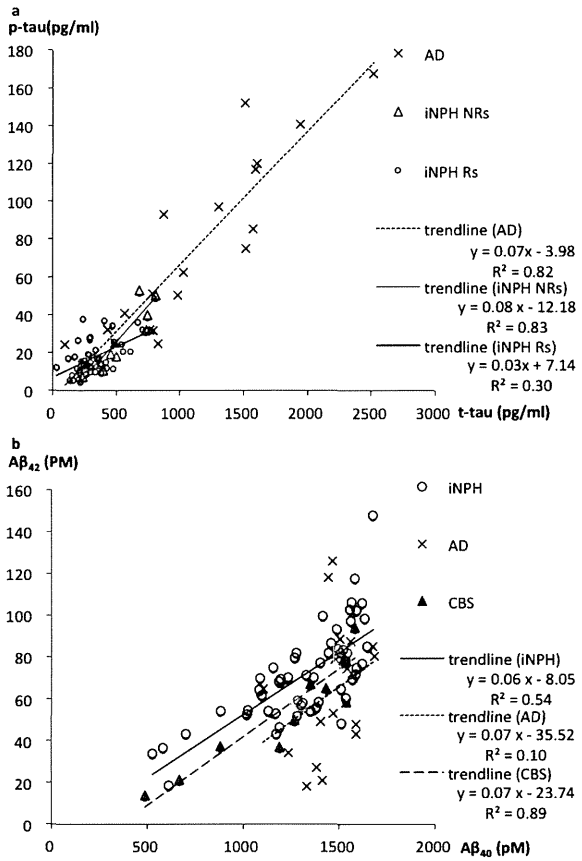

Fig. 3. Correlation between t-tau and p-tau in iNPH Rs, NRs, and AD (a). Correlation between $A\beta_{40}$ and $A\beta_{42}$ in iNPH, AD, and CBS (b).

the AD group (R = 0.26) (Fig. 3b). LRG levels did not differ among iNPH, AD, CBS, and SCD (Fig. 1d).

DISCUSSION

In this study, t-tau and p-tau levels were highly decreased in iNPH patients than in AD patients. Levels of t-tau and p-tau showed a strong correlation each other in AD, while they did not in iNPH Rs subgroup. Given that these two pathological conditions are distinguishable by differential biomarker profiles, iNPH appears to have a unique tau-negative pathology that differs from AD. In iNPH, an excessive volume of CSF, mainly accumulating in the cerebral ventricles and subarachnoid space of cortical sulci, might dilute the concentration of tau in CSF, which might account for the lower tau values. In iNPH Rs, t-tau levels were lower than those in NRs. Therefore, iNPH patients who have lower t-tau concentration in CSF might be the better candidates for surgical treatment.

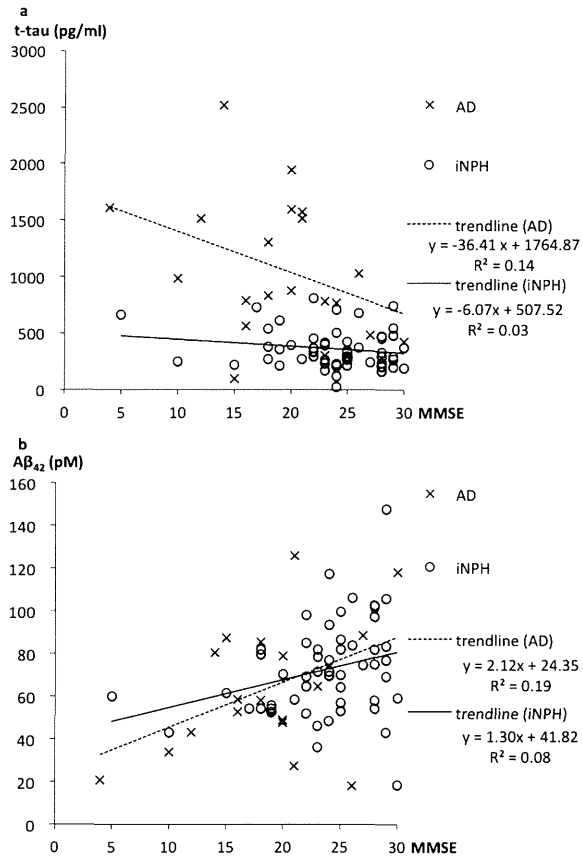

Fig. 4. Correlations between the MMSE score and t-tau (a) and $A\beta_{42}$ (b) in iNPH and AD.

The iNPH patients with higher t-tau and p-tau levels might have stronger overlaps of tau pathology such as AD. Another possibility is that the iNPH itself has progressed to an irreversible stage due to a longer clinical course, leading to severe white matter degeneration and neurodegeneration with higher average t-tau levels in CSF. Thus, iNPH patients with higher CSF t-tau values might have a progressive clinical course even after shunt surgery.

CSF $A\beta_{42/40}$ ratio in iNPH patients seemed to be significantly higher than in AD patients. We found a correlation between MMSE scores of iNPH patients and the levels of $A\beta_{42}$, which might suggest that the cognitive function of iNPH patients is affected by the preclinical stages of AD [14]. As there was a non-negligible MMSE score difference between the iNPH and AD groups ($p = 0.001$), we used ANCOVA with MMSE scores as a covariate for the evaluation of CSF $A\beta_{42/40}$ ratio between the two groups, resulting that the CSF $A\beta_{42/40}$ ratio does not statistically differ between iNPH and AD patients.

Interestingly, the profile in the levels of $A\beta_{40}$ and $A\beta_{42}$ in the AD group was different from those in the iNPH and CBS groups. In the groups of iNPH and CBS, the levels of $A\beta_{40}$ and $A\beta_{42}$ showed positive correlation; individuals with high $A\beta_{40}$ value in the CSF showed high $A\beta_{42}$ value as well. However, this correlation was not so clear in AD group. This might be explained by the preference for $A\beta_{42}$ deposition in the cerebral cortex of AD brain. The profile of $A\beta_{40}$ and $A\beta_{42}$ in iNPH group was similar to that in CBS group. This suggests that the amyloid pathology of iNPH as a group is discrete from that of AD as a group. The pathophysiology of iNPH does not seem to favor $A\beta_{42}$ deposition like AD.

The levels of LRG in CSF are reported to be increased in iNPH patients [11]. However, LRG levels were not different between iNPH and AD patients in this study. We also evaluated LRG levels between Rs and NRs iNPH patients, but could not find any difference. Since LRG is reported to be a potential biomarker for the diagnosis of iNPH, larger size of studies are required to evaluate the previously reported results.

The goal of our study is to search for useful CSF biomarkers to differentiate iNPH from AD. However, the comparison of CSF biomarker between iNPH and age-matched healthy control subjects was more ideal. Unfortunately, because the subjects were elderly patients, access to CSF samples from pure normal age-matched control subjects were limited in this study. The groups compared as control consisted of CBS and SCD. We chose to compare CBS patients because their levels of CSF tau are reported to not be increased [15], and they are not specific for amyloid pathology. Therefore, we assume that the quality of the compared groups including CBS were suitable for investigation of the biomarkers described above.

As iNPH NRs had higher CSF t-tau compared to Rs, and the cognitive function of iNPH patients was mildly associated with the level of CSF $A\beta_{42}$, it is true that some individuals in iNPH overlap with other neurodegenerative diseases, especially AD. The degree of overlapping pathology, which is clinically ineludible but difficult to be estimated, might be reflected by CSF biomarkers to a certain extent. The overlaps in CSF biomarker profile between these distinct pathological conditions may suggest that the pathophysiology of each iNPH individual is sometimes mixed and heterogeneous.

However, in conclusion, our results show that t-tau and p-tau were equally and highly useful CSF biomarkers for differentiating iNPH from AD, even though they might not specifically reflect the iNPH

pathophysiology. In addition, as in the two groups, the difference of Aβ profile shows discrete pathologies. The above biomarkers reveal that iNPH has a different CSF biomarker profile from AD. These CSF biomarkers could improve the diagnostic accuracy of iNPH, especially iNPH Rs with less tau pathology. They could also influence selection of the treatment course and could predict the prognosis of patients. The quest for more specific CSF biomarkers for iNPH is ongoing, and further studies should be conducted with in a larger population of patients.

ACKNOWLEDGMENTS

This work was supported in part by grants-in-aid from the Ministry of Education, Culture, Sports, Science and Technology of Japan, and the SRF (S.S.) and by an A-STEP grant from the Japan Science and Technology Agency (A.K.).

Authors' disclosures available online (http://j-alz.com/manuscript-disclosures/14-2622).

REFERENCES

[1] Adams RD, Fisher CM, Hakim S, Ojemann RG, Sweet WH (1965) Symptomatic occult hydrocephalus with "normal" cerebrospinal-fluid pressure. A treatable syndrome. *N Engl J Med* **273**, 117-126.

[2] Ray B, Reyes PF, Lahiri DK (2011) Biochemical studies in Normal pressure hydrocephalus (NPH) patients: Change in CSF levels of amyloid precursor protein (APP), amyloid-beta (Abeta) peptide and phospho-tau. *J Psychiatr Res* **45**, 539-547.

[3] Cabral D, Beach TG, Vedders L, Sue LI, Jacobson S, Myers K, Sabbagh MN (2011) Frequency of Alzheimer's disease pathology at autopsy in patients with clinical normal pressure hydrocephalus. *Alzheimers Dement* **7**, 509-513.

[4] Jack CR Jr, Vemuri P, Wiste HJ, Weigand SD, Lesnick TG, Lowe V, Kantarci K, Bernstein MA, Senjem ML, Gunter JL, Boeve BF, Trojanowski JQ, Shaw LM, Aisen PS, Weiner MW, Petersen RC, Knopman DS, Alzheimer's Disease Neuroimaging, Initiative (2012) Shapes of the trajectories of 5 major biomarkers of Alzheimer disease. *Arch Neurol* **69**, 856-867.

[5] Seppala TT, Koivisto AM, Hartikainen P, Helisalmi S, Soininen H, Herukka SK (2011) Longitudinal changes of CSF biomarkers in Alzheimer's disease. *J Alzheimers Dis* **25**, 583-594.

[6] Hu WT, Chen-Plotkin A, Arnold SE, Grossman M, Clark CM, Shaw LM, McCluskey L, Elman L, Karlawish J, Hurtig HI, Siderowf A, Lee VM, Soares H, Trojanowski JQ (2010) Biomarker discovery for Alzheimer's disease, frontotemporal lobar degeneration, and Parkinson's disease. *Acta Neuropathol* **120**, 385-399.

[7] Bech-Azeddine R, Hogh P, Juhler M, Gjerris F, Waldemar G (2007) Idiopathic normal-pressure hydrocephalus: Clinical comorbidity correlated with cerebral biopsy findings and outcome of cerebrospinal fluid shunting. *J Neurol Neurosurg Psychiatry* **78**, 157-161.

[8] Kapaki EN, Paraskevas GP, Tzerakis NG, Sfagos C, Seretis A, Kararizou E, Vassilopoulos D (2007) Cerebrospinal fluid tau, phospho-tau181 and beta-amyloid1-42 in idiopathic normal pressure hydrocephalus: A discrimination from Alzheimer's disease. *Eur J Neurol* **14**, 168-173.

[9] Agren-Wilsson A, Lekman A, Sjoberg W, Rosengren L, Blennow K, Bergenheim AT, Malm J (2007) CSF biomarkers in the evaluation of idiopathic normal pressure hydrocephalus. *Acta Neurol Scand* **116**, 333-339.

[10] Nakajima M, Miyajima M, Ogino I, Watanabe M, Miyata H, Karagiozov KL, Arai H, Hagiwara Y, Segawa T, Kobayashi K, Hashimoto Y (2011) Leucine-rich alpha-2-glycoprotein is a marker for idiopathic normal pressure hydrocephalus. *Acta Neurochir (Wien)* **153**, 1339-1346; discussion 1346.

[11] Li X, Miyajima M, Mineki R, Taka H, Murayama K, Arai H (2006) Analysis of potential diagnostic biomarkers in cerebrospinal fluid of idiopathic normal pressure hydrocephalus by proteomics. *Acta Neurochir (Wien)* **148**, 859-864; discussion 864.

[12] Relkin N, Marmarou A, Klinge P, Bergsneider M, Black PM (2005) Diagnosing idiopathic normal-pressure hydrocephalus. *Neurosurgery* **57**, S4-16; discussion ii-v.

[13] McKhann G, Drachman D, Folstein M, Katzman R, Price D, Stadlan EM (1984) Clinical diagnosis of Alzheimer's disease: Report of the NINCDS-ADRDA Work Group under the auspices of Department of Health and Human Services Task Force on Alzheimer's Disease. *Neurology* **34**, 939-944.

[14] Sperling RA, Aisen PS, Beckett LA, Bennett DA, Craft S, Fagan AM, Iwatsubo T, Jack CR Jr, Kaye J, Montine TJ, Park DC, Reiman EM, Rowe CC, Siemers E, Stern Y, Yaffe K, Carrillo MC, Thies B, Morrison-Bogorad M, Wagster MV, Phelps CH (2011) Toward defining the preclinical stages of Alzheimer's disease: Recommendations from the National Institute on Aging-Alzheimer's Association workgroups on diagnostic guidelines for Alzheimer's disease. *Alzheimers Dement* **7**, 280-292.

[15] Arai H, Morikawa Y, Higuchi M, Matsui T, Clark CM, Miura M, Machida N, Lee VM, Trojanowski JQ, Sasaki H (1997) Cerebrospinal fluid tau levels in neurodegenerative diseases with distinct tau-related pathology. *Biochem Biophys Res Commun* **236**, 262-264.

なぜ糖尿病患者にアルツハイマー病が高率に発症するのか

アルツハイマー病の発症・進展と耐糖能障害

The onset and progression of Alzheimer's disease from a viewpoint of glucose intolerance

前迫真人(写真)　木下彩栄
Masato MAESAKO and Ayae KINOSHITA
京都大学大学院医学研究科人間健康科学系専攻在宅医療看護学分野

◎糖尿病は孤発性アルツハイマー病(AD)の危険因子として注目を集めている．ADの初期病変である老人斑の形成は，発症の20年以上前から脳実質で起こる．したがって，老人斑形成と，その後の神経変性に至るそれぞれの過程を区別し，糖尿病が両過程にどのように影響するかを精査することは非常に重要である．近年，ヒトおよびモデルマウスを用いた研究から，耐糖能の異常が老人斑形成を促進することが明らかになりつつある．"先制医療"の重要性を考慮すると，耐糖能の異常と老人斑形成とを結びつける詳細な機序の解明は必要不可欠である．本稿ではADモデルマウスを用いた知見をもとに，とくに老人斑形成と耐糖能との関連性について，詳細な分子メカニズムに焦点を当てて考察したい．

Key word　老人斑，耐糖能，高脂肪食，BACE1

糖尿病はアルツハイマー病(Alzheimer's disease：AD)の後天的危険因子として注目を集めている．このことは，末梢臓器における恒常性の破綻が中枢神経系に影響しうることを示唆するものであり，"末梢から中枢"というあらたな概念を引き起こす点で非常に興味深い．海馬や大脳皮質の神経細胞外に沈着するβアミロイド(Aβ)凝集物(老人斑)は，もっとも初期に出現するADの病理変化であり，続いて，過剰にリン酸化したタウが神経細胞内に凝集する神経原線維変化，そして，神経細胞死が誘導される．一方，初期病変である老人斑の形成が，発症の20年以上前から脳実質で起こっていることを考慮すると[1,2]，ADにおいては一次および二次予防が重要である．したがって，①老人斑形成と，②その後の神経変性に至るそれぞれの過程に，糖尿病がどのように影響を与えるかを区別して精査することは非常に重要である．

本稿では，ADモデルマウスを用いた知見をもとに，とくに①の老人斑形成と耐糖能との関連性について，詳細なメカニズムに焦点を当てて考察したい．

耐糖能と老人斑形成に関する疫学研究

オランダのRotterdam Studyを筆頭に多くのコホート研究が，ADの発症リスクを糖尿病が高めることを支持している[3-6]．しかし，糖尿病の診断基準に調査間でばらつきがある点や，長年ADの鑑別に神経心理的分類に主眼をおくNINCDS-ADARAが用いられてきた点など課題も残る．

わが国における久山町研究は，神経病理学的所見も取り入れた疫学研究であり，耐糖能の異常が老人斑形成に関与する可能性を示唆する特筆すべき研究である．小原らの報告によると，1998年WHO分類による正常群に比べ，糖尿病群でADの発症リスクが2.1倍高まること，一方で，空腹